THESIS

ENERGETICS AND DYNAMICS OF FLOW THROUGH BAFFLE DROP SHAFTS USING PHYSICAL AND COMPUTATIONAL MODEL STUDIES

Submitted by

Kasun Prabodha Sahabandu Aluthwalage

Department of Civil and Environmental Engineering

In partial fulfillment of the requirements

For the Degree of Master of Science

Colorado State University

Fort Collins, Colorado

Summer 2023

Master's Committee:

Advisor: Subhas Karan Venayagamoorthy
Co-Advisor: Ho Huu Loc

Peter Nelson
Bret Windom

ABSTRACT

ENERGETICS AND DYNAMICS OF FLOW THROUGH BAFFLE DROP SHAFTS USING PHYSICAL AND COMPUTATIONAL MODEL STUDIES

A drop shaft is one of the main hydraulic structures that is used to convey water from higher to lower elevations while dissipating potential energy in storm water management systems, water treatment plants, and hydropower stations. Drop shafts need to be adjusted for higher discharges because of the increased urban flooding due to climate change and rapid urbanization. Traditional baffle drop shafts have limited flow capacity and are unstable due to their asymmetric nature. The novel baffle drop shaft is proposed here for larger range of flow discharges. To the author's knowledge, there are no previous studies that have thoroughly investigated the energy dissipation potential of the novel baffle drop shaft. Hence, there is a need to establish a design relationship between key parameters such as the shaft diameter, baffle spacing, and discharge to inform best design practices.

A 1:10 physical model study was carried out to investigate the energy dissipation of a novel baffle drop shaft using different discharges. Pressure and velocity were measured at two locations on the baffles using low range pressure sensors (100 mbar) and an electromagnetic velocity meter. Timed averaged pressure and velocity on the baffles increased with discharge. These averaged quantities were considered to calculate global and local energy dissipation through the shaft. The global energy dissipation efficiency was calculated based on the inlet and outlet channel flow data, and was found to range from 89.6% to 91.9%. The flow regime profiles were quite similar on each baffle section of the shaft; hence, we can consider the energy dissipation in each baffle to be equivalent. Under free-flow conditions, the energy dissipation efficiency decreases as the discharge increases.

Physical models are costly and time-consuming for performing parametric studies of flow through such structures because each and every geometric configuration needs to be constructed in the lab. Computational Fluid Dynamics (CFD) is a more feasible option to conduct an in-depth investigation of the energetics and dynamics of flow in a baffle drop shaft since it is faster and more cost-effective than a physical model study. The CFD models have been built to simulate the hydraulic behavior of baffle drop shafts using OpenFOAM. This software is adaptable for modeling diverse flow issues due to the variety of models and numerical techniques that it incorporates. A suitable turbulence model that is commonly used in CFD for modeling turbulent flows such as in drop shafts is the RANS-based realizable k- ϵ model. Mesh sensitivity analysis was also performed to establish grid independences of the solution.Benchmark geometry CFD models were calibrated using four locations in the physical model, and velocity and pressure measurements at the edge of the baffle were used for validation with remarkable agreement.

A parametric study was conducted using shaft diameters (D) of 0.8 m, 0.9 m, and 1 m, six baffle spacings (h) ranging from 0.23m to 0.48 m, and baffle rotating angles (θ) of $180°$, $250°$, and $270°$. Global energy dissipation efficiency (η) ranged from 92% to 97%. The η value decreased with discharge but was higher under free flow conditions in the baffle drop shaft. The geometric parameters D, h, and θ have little influence on energy dissipation. Considering structural integrity, available space, construction costs, and maintenance costs, the baffle drop shaft needs to be optimized to achieve the desired hydraulic performance. Maximum pressure was observed at the water jet impact location close to the outer shaft wall. Air entrainment is also a significant consideration in designing baffle drop shafts because its impact is critical in applications like hydro power generation. The bulking of the flow due to air entrainment needs to be considered to evaluate the maximum flow carrying capacity of baffle drop shafts. In summary, designing baffle drop shafts requires a multi-criteria approach that is mainly dependent on the design requirements on energy dissipation, structural integrity, construction costs, air entrainment, application, and location.

ACKNOWLEDGEMENTS

I would like to express my sincere gratitude to everyone who has been part of my journey in completing my thesis. It would have been much difficult without the help of all these people. First, I express my sincere gratitude and appreciation for the guidance and opportunities for growth provided to me by my advisor, Prof. Karan Venayagamoorthy and co advisor, Dr. Ho Huu Loc for their continuous support and guidance throughout my MS journey. I am also grateful to Dr. Bret windom and Dr. Peter Nelson who serve on my MS thesis committee from Colorado State University (CSU), and Prof. Sangam Shrestha and Dr. Mohana Sundaram Shanmugam from Asian Institute of Technology (AIT) who serve on my examination committee, for their comments and contributions.

I would like to thank you Mr. Artuto Roa and Mr. Soupote from Water Engineering and Management (WEM)at AIT for sharing their knowledge and support for the physical modeling study.

I also wish to thank my family; father, mother, brother and sister for their unwavering support. I wish to express my appreciation to my friends at both CSU and AIT for being my family away from home.

Finally, I would like to acknowledge the Department of Civil and environmental engineering at CSU and Asian Institute of Technology for providing me with scholarships and giving me the opportunity to obtain my master's degree.

TABLE OF CONTENTS

LIST OF TABLES

LIST OF FIGURES

Chapter 1

Introduction

1.1 Background and Motivation

Water is one of the main driving forces in human civilization. People have stored and conveyed water based on their requirements since ancient civilizations like Mesopotamia, the Incan, Egypt, India, China, Rome, and Greece. Hydraulic structures that they used to convey water were vulnerable to damage due to high impact forces caused by the flow. Hence, energy dissipation is crucial in water conveyance systems especially when there is an elevation drop. Energy dissipation and drop structures were used in ancient civilizations like the Romans more than 3000 years ago [4] . Other civilizations also used drop structures as well as energy-control mechanisms in irrigation schemes and drainage systems. These drop structures are used as multipurpose structures. For example, Roman drop shafts acted as sediment traps, and "Biso Kotuwa", which was a water-releasing gate in ancient tanks in Sri Lanka, was used as a surge tank. The main hydraulic drop structures that convey water from higher elevations to lower elevations are drop shafts. Currently, drop shafts are used in storm water conveyance systems, water treatment plants, and hydropower stations.

Due to climate change and rapid urbanization, urban floods have increased significantly as a result of the depletion of pervious lands. Rainfall infiltration has reduced as impermeable areas have increased, resulting in a shorter rainwater runoff time and a huge increase in runoff and peak discharge. Dealing with such large discharges becomes one of the main challenges in the storm water management system. Deep tunnel drainage has gradually become the primary method for large towns to deal with flood disasters with large discharges [5]. Drop shaft structures convey water from shallow drainage systems to deep tunnels or underground storage. The purpose of a drop shaft in a hydroelectric conveyance system is to dissipate energy from the falling flow while minimizing air entrainment. It helps protect turbines from high-impact energy, air entrainment, and cavitation.

The applicability of different types of drop shafts mainly depends on the purpose, location, and energy dissipation mechanism. There are four types of drop shafts used in storm water management systems and hydropower namely: simple plunge drop shafts, vortex drop shafts, baffle drop shafts, and step spillway drop shafts [6]. The basic drop shaft is a simple plunge where the flow plunges into the water chamber with minimum energy dissipation. Vortex drop shafts were introduced to handle larger discharges. As a result of its excellent energy dissipation capacity and its adaptability to a wide range of inflow conditions, the baffle drop shaft has been widely used in deep tunnel drainage systems, but it requires a larger area than the vortex drop shaft. A step spillway drop shaft is introduced to deal with large discharges compared to the traditional baffle drop shaft. An example of water falling into a drop shaft is shown in Figure 1.1.

Figure 1.1: Circular water jet falling down into the energy dissipation chamber (Photo: Hohl)

The flow dynamics through drop shafts were investigated in different research studies by changing their design parameters. Most of the studies used physical models, numerical models, and a combined approach to study the hydraulics of drop shafts. Baffle drop shafts have significant characteristics compared to other drop shafts: less drop height, relatively low velocity, less erosion potential, and low air entrainment. When the flow cascades down the shaft from one baffle to the next, there is a plunge on each baffle, which distinguishes a baffle-drop shaft from other types of drop shafts. The flow dynamics of the baffle drop shaft can be investigated using numerical model studies, after validation with physical model experiments.

The traditional baffle-drop structure is separated into a dry side and a wet side by a vertical partitioning wall that runs the length of the structure. The baffles are placed on the wet side [7]. Traditional baffle drop shafts have limited flow capacity and are unstable due to their asymmetric nature. The novel baffle drop shaft is proposed for large-range flow discharge with a symmetric structure; hence, it is structurally stable and directly uses the construction shaft as part of the structure. There are no clear guidelines for designing novel baffle drop shafts. Hence, there is a need to study the flow dynamics and establish design relationships between key parameters such as shaft diameter, baffle spacing, and discharge.

Establishing relationships between design parameters and improving structural stability of baffle drop shafts is a novel study area, and there is a need to develop methodologies and techniques for the investigation of flow characteristics and energy dissipation. Most of the previous baffle drop shafts were designed based on prior experience with other types of drop shafts but the literature is limited on this topic. The inlet and outlet conditions of the drop shaft may vary based on a particular application. Drop shafts need to be studied from energy dissipation, air entrainment, maximum discharge, and velocity perspectives. There are two types of novel baffle drop shafts.

- Type 1 - Wet zone is inside and dry zone is outside.
- Type 2 - Dry zone is inside and wet zone is outside.

Even though type 2 could accommodate larger discharges, no studies have thoroughly investigated its energy dissipation potential. Energy dissipation is one of the main criteria in baffle drop

shaft design because it directly relates to high impact energy, large pressure fluctuations, and high local fluid velocities. An investigation of flow dynamics can be determined via the use of a physical model. However, this method is not only expensive but also time-consuming; thus, computational fluid dynamics (CFD) models might be utilized to run more test configurations after validation them using results from the physical model study. CFD is a simulation technique that combines fluid mechanics and numerical methods to simulate fluid flow under specified conditions. The study presented in this thesis uses both a physical model experiments and CFD to investigate the flow dynamics of a novel baffle drop shaft.

1.2 Objectives

It is essential to understand the hydraulic performance of baffle drop shafts in terms of their ability to dissipate energy dissipation and ensure structural integrity. The primary goal of this thesis is to investigate the energetics and dynamics of type 2 baffle drop shafts in a reliable and scientific manner. A hybrid method of physical modeling and CFD is a suitable approach because the limitations of each method can be reduced using the combined approach. The set of objectives of this thesis are as follows:

1. To conduct a scaled physical model study of flow through a type 2 novel baffle shaft to gain insights into the flow dynamics and evaluate energy dissipation.

2. To calibrate and validate CFD model using physical model measurements.

3. To evaluate how energy dissipation, pressure distributions and water depth vary with discharge and different geometric configurations of baffle drop shafts.

1.3 Thesis Outline

The thesis outline is as follows. In Chapter 2, a review of the relevant literature related to baffle drop shafts, physical models, CFD models, energy dissipation, structural aspects, and dimensional analysis is presented. Chapter 3 focuses on the physical model study conducted as part of this

research. This includes model scale selection, instrumentation and measurement of velocity and pressure, and evaluation of global energy dissipation. Chapter 4 presents the CFD model study that includes an extensive parametric study of the baffle drop shaft with an emphasis on evaluating the global and local energy dissipation, pressure distributions, and the bulking effects of water due to air entrainment. Chapter 5 concludes with a summary of relevant findings and recommendations for future work.

Chapter 2

Literature Review

This chapter provides a review of baffle drop shafts, their applicability, and parameters that influence the energy dissipation of baffle drop shafts. Drop shafts have been used throughout history, from early civilizations through modern-day deep tunnel drainage systems. The design and construction of drop shafts have evolved over time to improve their efficiency and effectiveness in controlling water flow based on their purpose and application. To determine the scope of existing research, a synthesis of previous studies on baffle drop shafts is presented. A review of physical models and computational fluid dynamics (CFD) models is also conducted to evaluate flow dynamics through a baffle drop shaft.

2.1 Drop Shaft

Drop shaft structures are used to convey water from a higher elevation to a lower elevation in storm water management systems, waste water treatment plants, and hydropower plants. Many drop structures that have been in use for a long time have deteriorated and incurred severe damage, due to high impact forces of the free falling water over a high elevation difference or defective construction [8]. The hydraulics of the drop need to be understood for different flow configurations, mainly free flow, and pressurized flow (pipe flow) conditions, based on a given application. As mentioned earlier, extensive work has gone into understanding the drop shafts due to important applicabilions in drainage and tunnel systems.

Drop shafts are frequently utilized in civil engineering for a number of applications, including irrigation systems, wastewater treatment, stormwater management, and hydropower. They are designed to regulate water flow in order to reduce down erosion and damage to structures further downstream. These deep tunnel drainage systems are used in many parts of the world, like the Tunnel and Reservoir Plan System in Chicago, the "Sponge City" program in China, and the deep sewer network in Edmonton, Canada [5, 9]. Stormwater discharges have increased due to rapid

urbanization and climate change. Hence, deep drainage systems are used for flood control by diverting water to underground tunnels and storage. These drop systems often have depths ranging from less than 15 meters to well over 60 meters and are traditionally defined by having several vertical shafts [5, 6].

Drop shafts are used in water treatment plants for conveying and controling flow. To eliminate instabilities and provide smooth transitions between air-entrained flow modes and full-pipe operation modes, drop shafts in treatment plant make use of an air intake control system that is self-activating, non-powered, and does not contain any moving parts. [10]. The energy dissipation of the flow needs to be maximized to maintain low velocity flow in the treatment plant's conveyance system. This is usually accomplished when transferring water from a high elevation to a lower elevation by dissipating the available potential energy. The stability of the drop-shaft chamber's flow and discharge sections is critical for the following reasons: Large-scale surges in the lower conduit system originate from uncontrolled discharge from the sump chamber without de-energizing the flow. The combination of this surge and the entrainment of significant amounts of air will have an impact on downstream operations. Therefore, there is a critical the need to focus on energy dissipation and air entrainment especially in hydropower stations [8, 11]. For example, turbines can fail due to high impact energy, cavitation, and air entrainment when conveying water [12].

2.2 Evolution of drop shaft designs

Different methods and structures for managing and controlling the flow of water for agricultural, industrial, and home uses have been developed by human civilizations across time. Based on changing demands, knowledge, and technical developments over time, these structures have changed and improved. The development of drop shafts began in the early 19th century and have since evolved. More complex drop structures are now in use mainly due to improvements in computer modeling, materials, and building methods. Environmental considerations and sustainability have become important factors in the design and construction of drop structures. There are mainly four types of drop shafts currently in use, namely;

- Simple plunge drop shaft
- Vortex drop shaft
- Baffle drop shaft
- Stepped drop shaft

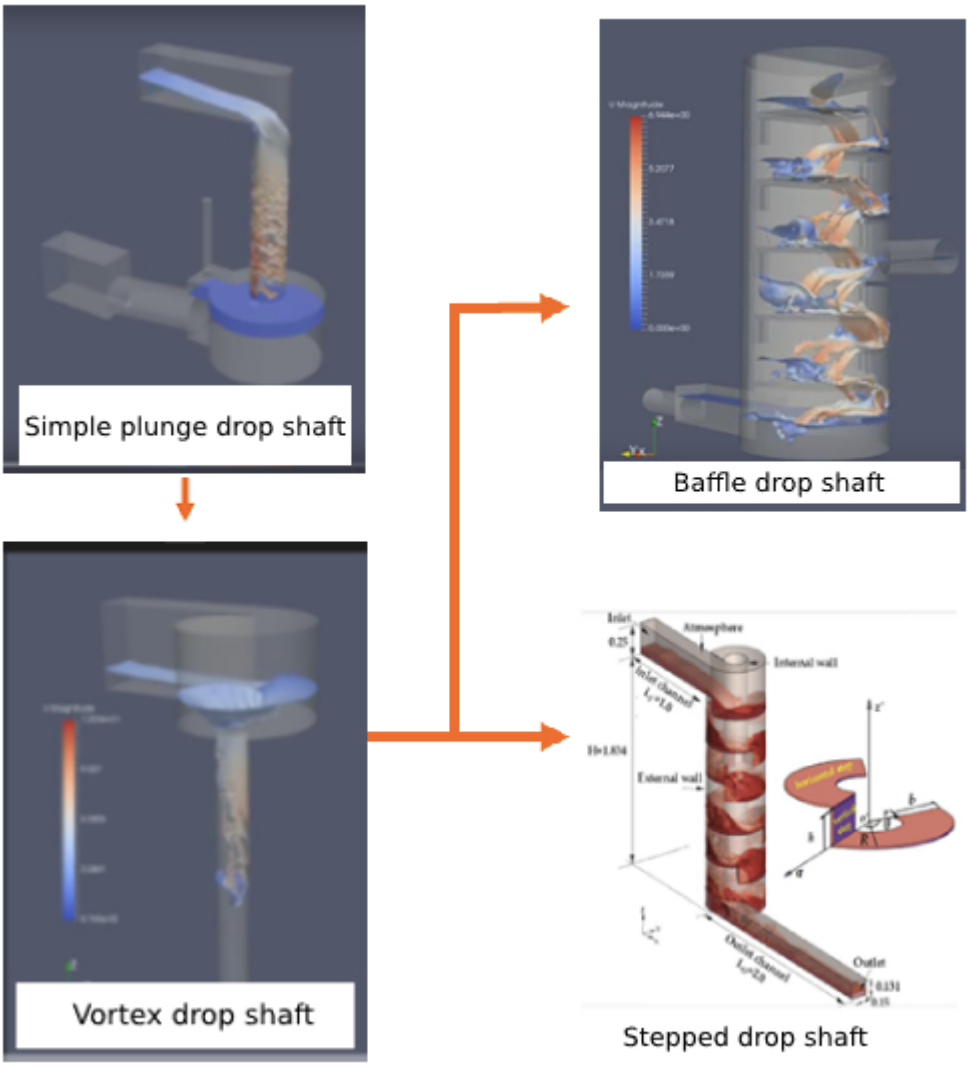

Figure 2.1: Evolution of drop shaft (Source - YouTube and [1]

The evolution of the drop shaft can be summarized according to the Figure 2.1. The baffle and stepped drop shafts have been developed to convey water much deeper and minimize the pressure on the bottom of the shaft. These drop shafts are different due to varying geometrical features. A simple plunge drop shaft consists of a vertical pipe or shaft without special inlet conditions, any internal structures or baffles to dissipate energy and reduce turbulence. Water drops vertically into a lower chamber or tunnel. A hydraulic device used in urban sewage systems to control wastewater flow is called a vortex drop shaft. It is made to slow down incoming wastewater flow and produce a vortex flow pattern that aids in separating particulates from liquid stream. This structure is often put in place when a sewer pipe flows into a bigger sewer or treatment facility. Vortex drop shafts are being used more frequently because of their capacity to handle significant discharges [13].

A baffle drop shaft is a type of energy dissipation structure that consists of a vertical shaft with several staggered baffles installed inside. The water cascades down the structure from baffle to baffle and plunges into a pool at the bottom to dissipate the energy of the water flow and prevent erosion. The baffle drop shaft is divided into two zones by a partition: the wet zone, which contains interlaced baffles and serves as the water flow passage, and the dry zone, which contains vent holes arranged on the partition to connect it with the wet zone. The vent holes allow air to exchange between the dry and wet zones, to help reduce pressure inside the drop shafts. Baffle drop shafts are commonly used in combination with other structures, such as stilling basins and plunge pools, to provide effective energy dissipation and prevent damage to downstream infrastructure [2]. A stepped spillway drop shaft was constructed out of a number of steps that divide the water flow and absorb its force, lowering the possibility of erosion and damage downstream. To improve the drop shaft's performance under various flow circumstances, it is possible to change the height, angle, and height of the steps ([14]). The main advantage of baffle drop shafts and stepped drop shafts is that they require minimum air entrainment and can deal with higher discharges than simple plunge and vortex drop shafts, but they require a larger area and a higher construction cost.

2.3 Traditional Baffle Drop Shaft and Novel Baffle Drop Shaft

A baffle drop shaft was proposed by Margevicius [15] for sewage conveyance in York Region, Ontario. In a traditional baffle-drop shaft, a vertical partitioning wall splits the shaft into a dry and wet zone, and baffles are located in the wet zone. The dry zone allows for surge mitigation and maintenance. Each and every baffle consists of an inspection port underneath it, which allows for the exchange of air between two zones. Baffle drop shafts can deal with larger discharges than simple plunge and vortex drop shafts with minimum air entrainment. Only a few available studies on baffled shafts have been conducted. Due to limited flow capacity and the instability of the asymmetric structure of traditional baffle drop shafts, a novel baffle drop shaft with a symmetric structure was proposed by Wang [2]. Fiure 2.2 shows schematics of both the traditional baffle drop shaft and a novel baffle drop shaft. One of the main advantages of the novel baffle drop shaft is that it uses the construction shaft as the outer wall of the drop structure. The majority of previous research on baffle drop shafts focused on their use in drainage and sewage systems with respect to discharge capacity and energy dissipation.

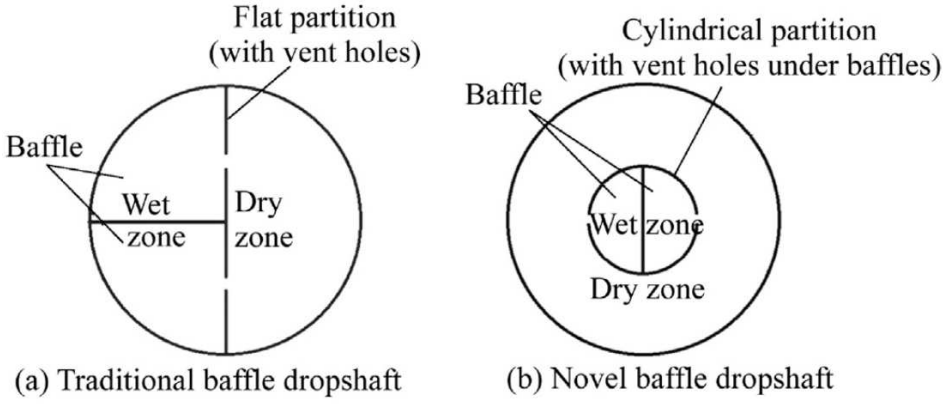

Figure 2.2: Schematic diagram of plane structure of traditional and novel baffle drop shafts. Fig 1 in [2]

Margevicius [15] focused on discharge and baffle spacing for his study and found that baffle drop structures are an effective method for dropping large amounts of flow from multiple sources into deep tunnels compared to other drop structure types. One of the other notable works was done

by Stirrup (2012), where they considered discharge, baffle spacing, the location of the dividing wall, and the location of the inspection port. Odgaard [7] conducted a series of experiments to establish a design relationship between discharge, baffle spacing, position of the dividing wall, and baffle thickness using a 1:19.7 physical model. The energy dissipation rate of the drop shaft decreased with the increase in the inflow discharge, and the energy dissipation rate was found to range from about 63.14% to 96.40% by Yang and Yang [6] using a 1:25 scale model.

Yang and Yang [16] developed a CFD model of a traditional baffle drop shaft using ANSYS Fluent and validated their results from their previous physical model study in 2020. Baffles play a major role in the energy dissipation of the drop shaft at low flow rates, but at high flow rates, the energy dissipation is mainly achieved via the baffles and the shaft bottom. A baffle spacing that is too dense or too sparse is not conducive to energy dissipation and discharge, according to Yang and Yang [16]. Wang [2] obtained a similar result about energy dissipation rate and discharge, even though they used a novel baffle drop shaft. Global (overall) energy dissipation rate decreases with the increase in flow rate in both traditional and novel baffle drop shafts. Discharge, baffle spacing, shaft diameter, baffle width, position of the dividing wall, location of the inspection port, baffle thickness, and baffle angle are the main design parameters of baffle drop shafts. The maximum operating capacity increased with baffle spacing , and energy dissipation also depended on these parameters [6].

2.4 Energy Dissipation

Baffle drop shafts must be protected from high impact energy, which necessitates maximizing energy dissipation to avoid structural damage and protect downstream equipment. Friction between the water flow and the surfaces of the baffles and shaft walls, breakdown and coalescence of the water flow, and the viscosity effect of the flow fluid can all be energy dissipation mechanisms in baffle drop shafts [16]. Table 2.1 illustrates the different energy dissipation efficiencies for a number of different drop shafts.

The majority of the studies that have been done on baffle drop shafts have mainly concentrated on the hydraulic characteristics and energy dissipation [15]. The principal energy dissipation process in a baffle drop shaft is the impact of the water on each baffle as the flow cascades down the shaft. The energy is further dissipated through friction between the water and the surfaces of the drop shaft, as well as the processes of water breakup and coalescence.

Table 2.1: Energy dissipation efficiency comparison.

Type of Drop Shaft	Energy Dissipation Efficiency (η)	Reference
Plunging Drop Shaft	85% - 95%	N. Rajarathnam (1997) [17]
Vortex Drop Shaft	η>90%	G. Crispino (2021) [18]
Stepped Spillway Drop Shaft	Without end sills – 86.79% - 96.42% With end sill – 91.22% - 96.4 %	SHEN JieYi (2019) [14]
Baffle Drop Shaft (Type 1)	63.14% - 96.4%	Q.Yang and Q. Yang (2020) [6]

The novel baffle drop (Type 1) shaft's baffle spacing has less impact on the overall energy dissipation rate, but it has a stronger impact on flow patterns and baffle pressure distributions [2]. The majority of research were conducted under steady-flow conditions. In reality, the majority of baffle-drop shafts operate in unsteady flow conditions, and the varied inflow discharge will have a substantial effect on the baffle construction [6]. However, the relationship between the type 2 novel baffle drop shaft's parameters and the energy dissipation have not been established as yet.

2.5 Physical Models

A physical model is a scaled representation of a hydraulic flow scenario while fulfilling boundary conditions. The common force ratios used in checking for model similitude are the Froude number (Fr), Reynolds number, and Weber number. Fr is the ratio of inertial to gravitational forces and it is defined in equation (2.1). The Reynolds number (Re) is the ratio of inertial to viscous forces, and the Weber number (We) is the ratio of inertia to surface tension forces. However, it is challenging to achieve similarity of both Re and Fr. The surface tension effects are likely to

be negligible in such flows. Given the dominance of free surface effect, Fr similitude is sought while ensuring that both Re and We are sufficiently large by using a a suitable model scale [19].

$$Fr = \frac{V}{\sqrt{gh}}, \tag{2.1}$$

where V is the flow velocity, g is the acceleration due to gravity and h is the water depth. Typical model scales selected by previous researchers were between 12.5 to 25. Energy dissipation and air entrainment are entangled in the sense that entrainment does result in significant energy losses. Hence, a physical model needs to provide a good and reliable representation with adequate dimension. With some simplifications, laboratory models can be used effectively to model the full-scale problem. Guidance based off of previous experimental studies on drop shafts suggest that the model scale must not exceed 1:10, and the flow through the model needs to have $Re > \mathbf{1x10^5}$ and $\mathbf{We} \geq \mathbf{32}$ [19].

Table 2.2: Scale ratios used in physical model based on Fr similitude.

Parameter	Scale Relation
Length	$\mathbf{L_r = L_p/L_m}$
Velocity	$\mathbf{V_r = (L_r)^{1/2}}$
Discharge	$\mathbf{Q_r = (L_r)^{5/2}}$
Roughness	$\mathbf{n_r = (L_r)^{1/6}}$
Pressure head	$\mathbf{h_r = L_r}$

The baffle drop shaft model will be constructed to a geometric ratio ($\mathbf{L_r}$). where $\mathbf{L_m}$ is the characteristic length in the model and $\mathbf{L_p}$ is that in the prototype. The scalings of pertinent variables based on Fr similitude is shown in Table 2.2.

2.6 Computational Fluid Dynamics (CFD)

Computational fluid dynamics is the mathematical modeling and numerical solution of a physical phenomenon involving fluid flow using computer power. Essentially, the Navier-Stokes (conservation of momentum) equations (equations 2.2) are solved together with the conservation of mass (continuity) equation (equation 2.3) numerically in CFD models to obtain the velocity and pressure fields in the computational domain of interest [20].

$$\frac{\partial \mathbf{u}}{\partial t} + (\mathbf{u} \cdot \nabla)\mathbf{u} = -\frac{1}{\rho}\nabla p + \nu \nabla^2 \mathbf{u}, \tag{2.2}$$

$$\nabla \cdot \mathbf{u} = 0, \tag{2.3}$$

where:

$\mathbf{u} = (u, v, w)$ is the velocity vector,

t is time,

p is pressure,

ρ is density,

ν is kinematic viscosity.

To facilitate access to their problem-solving capabilities, all commercial CFD software include sophisticated user interfaces for inputting problem parameters and examining the results. Therefore, all codes contain the following three elements: (i) a pre-processor, (ii) a solver and (iii) a post-processor [21]. Pre-processing is entering a flow problem into a CFD program using a user-friendly interface, and then converting this input into a format that the solver can use. Almost always, the governing equations describing fluid motion and physics are too complex to solve analytically. Typically, they are composed of distinct partial differential equations that can be coupled or of various types of derivatives. To actually solve these equations, they are discretized so that

they can be solved numerically on a computational mesh. CFD solvers employ three prevalent solution methods: finite difference, finite element and spectral methods. Post-processing in CFD refers to the analysis and visualization of simulation results after the simulation has been completed. It involves using software tools to extract and analyze data from the simulation output files, and then presenting this data in a way that is easy to understand.

Due to the complexity of the mathematical models, there are still various hurdles in the exploration of multiphase flow. The following are the most frequently utilized mathematical approaches to investigate multiphase flows.

- Volume of Fluid (VOF)
- Eulerian Multiphase (EMO)
- Lagrangian Multiphase (LMP)
- Eulerian/Lagrangian Dispersed Phase Model (DPM)

2.6.1 Volume of Fluid (VOF)

VOF and Eulerian models are commonly used to represent two-phase flow [3]. A separate momentum and energy equation are solved for each phase in an Eulerian model while sharing common pressure fields. The VOF technique examines all phases by applying a single equation to each transport phenomena [22] and it is a simplified version of the full Eulerian model for continuous – continuous phase interaction. The Eulerian model takes much longer to simulate than the VOF model using the same number of cells and in the case of bubbly flow, the Eulerian model is 5% more accurate than the VOF model in predicting void fraction [3]. If higher number of cells are used, the errors become similar between Eulerian and VOF method as shown in Figure 2.3. Performing grid independence tests to find optimum number of cells using VOF method is a good option to simulate baffle drop shafts.

The VOF technique is used to determine the free surface between air and water, which are both regarded as incompressible fluids with no mass or heat exchange. The free surface is modeled by

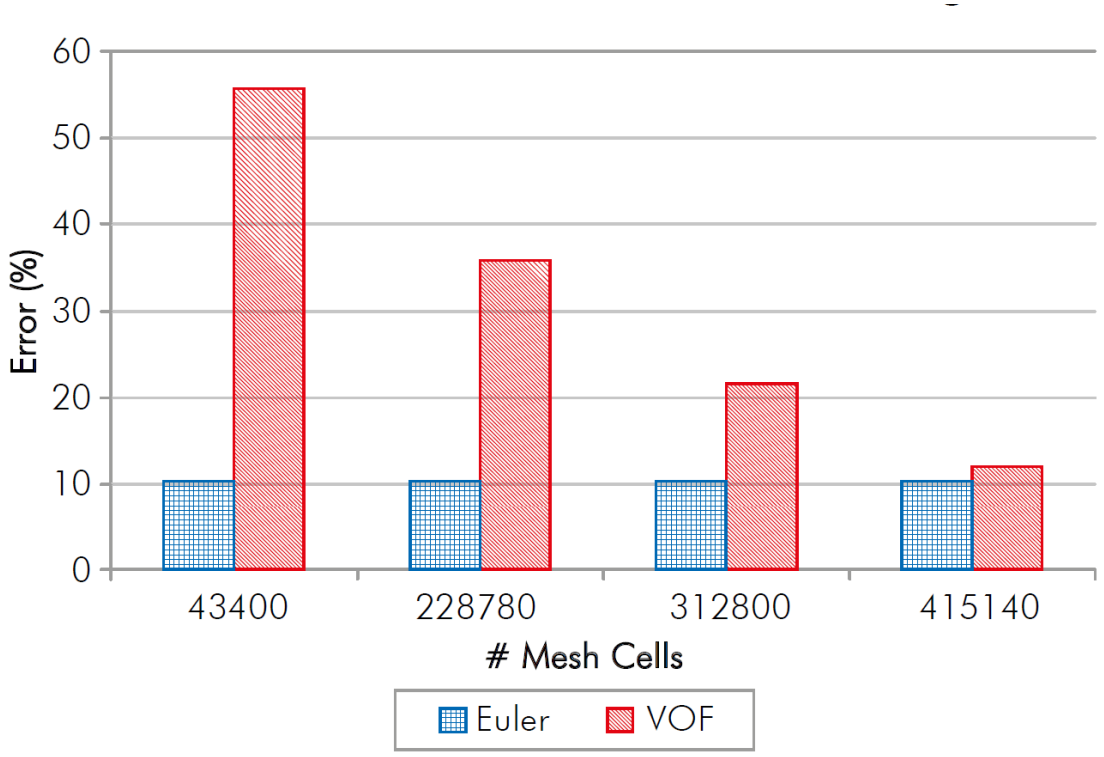

Figure 2.3: Error change with respect to number of mesh. Fig 4 in [3]

introducing a function α that is defined to be unity at any location completely filled with water and zero where there is only air.

2.6.2 Turbulence models in CFD

Many practical fluid flow problems must also take turbulence into account. Flow characterized by irregularity, nonlinearity, dissipation, vorticity, and diffusivity constitutes turbulence. Its intricacy makes it extremely difficult to recreate in a computational model, and its susceptibility to minute changes makes it impossible to reproduce experimental results precisely. The complexity of solving the Navier–Stokes equations lies predominantly in the solution for the turbulence of the flow. A number of various turbulence models are available. Turbulence must be correctly modeled in order to produce accurate and trustworthy CFD results. Direct Numerical Simulations (DNS), Large Eddy Simulation (LES) Unsteady Reynolds Average Navier-Stokes (URANS) and Reynolds Average Navier-Stokes (RANS) are some of the turbulence models that are commonly used in CFD [23].

Direct Numerical Simulation is referred to as DNS. It is a computational fluid dynamics (CFD) method that does not use turbulence modeling but instead solves the Navier-Stokes equations directly. By resolving all scales of motion, from the largest to the smallest, DNS offers the most accurate simulation of fluid flow, but it is computationally expensive and needs high-performance computing resources. In research, DNS is employed to examine fundamental issues of turbulence and fluid mechanics. Large Eddy Simulation (LES) models the smaller-scale structures while solving the Navier-Stokes equations for the large-scale turbulent structures in a flow. LES is more accurate than RANS (Reynolds-Averaged Navier-Stokes) simulations and less computationally expensive than DNS. Reynolds-Averaged Navier-Stokes (RANS), the most popular and least computationally expensive turbulence model, comes next. RANS is an all-encompassing word that encompasses a number of different models. But they all share a lot of traits in common. The RANS models employ a time filter, whereas the LES models utilize a spatial filter. RANS simulations rely on turbulence models to take into account the effects of turbulence on the flow, although being less computationally expensive than LES and DNS [21].

The computing cost of a CFD simulation rises from RANS to DNS because of the number of degrees of freedom needed to solve the flow. In baffle drop shaft, we mainly focus on predicting the water surface because it relates to surface elevation. RANS model predict free surface better than LES model with respect to time and frequency domain [24].

RANS models can be divided into linear eddy viscosity models and nonlinear eddy viscosity models. One of the most popular RANS turbulence models is the two equation turbulence model, which is a linear eddy viscosity model. k – ω (Turbulent kinetic energy, k and energy in the turbulence, ω) and k – ϵ (Turbulent kinetic energy, k and turbulent dissipation, ϵ) are based on the RANS model [23]. The k – ϵ model provides more turbulence details based on flow domain [25] and has lower computational cost than k – ω model . There are three major formulations of k – ϵ models, namely Standard k – ϵ model, Realizable k – ϵ model and Re-Normalization Group (RNG) k – ϵ model. The RNG k - ϵ model was created utilizing a rigorous statistical technique in order to take into account different scales of turbulent motion by varying the production term [26]

The flow conditions in novel baffle drop shaft are turbulent with strong vorticity due to the complex swirling flow structure [2]. RANS realizable k – ϵ can determine baffle jet divergence and calculate complex flows like rotational shear flow and free flow with good computation efficiency [23, 27–29]. The realizable k – ϵ model is, by definition, mathematically realizable in all cases. When the mean strain rate of the flow is extremely high, the standard and RNG - models exhibit mathematical anomalies. The realizable - model accounts for these anomalies by solving for C $_\mu$, a model coefficient based on the flow's turbulence, such that there are no mathematical anomalies and the equations are always realizable. Validation indicates that the realizable model outperforms the other models in situations involving separated flows and flows with intricate secondary flows.

2.6.3 Meshing

Mesh generation is a required step in most CFD applications. Choosing the proper mesh, applying the right density to crucial locations, and picking the right coarseness or looseness all have an impact on the simulation's accuracy and speed. The mesh elements/cells are generally hexahedral, tetrahedral, square pyramids or polyhedral. Hexahedral meshes have the advantage of being able to be subdivided anisotropically several times without losing element quality [30].

2.6.4 CFD software

There are more than a hundred CFD related software and can be categorized into solvers, grid generation software, visualization software, and solver couplings. The software can be further categorized into CAD Embedded, Open-Source, Semi-Comprehensive, and Comprehensive. OpenFoam, ANSYS, COMSOL, and Flow 3D are some examples of CFD platforms. OpenFOAM is an open source platform that includes a number of C++ libraries. ANSYS Fluent and Flow 3D are widespread CFD solvers [31]. OpenFOAM is able to simulate multiphase fluid flow in a free-surface state, which consists of two miscible liquid phases with varying temperatures and densities [29]. The main advantage of OpenFoam is its availability as an open source CFD code.

Most Linux operating systems support the OpenFOAM package, and Mac OS versions are also available. Running OpenFOAM on Windows is possible with a Linux subsystem. Within

the RANS, LES, and DNS simulation/modeling frameworks, OpenFOAM is distributed with a vast number of models, including laminar and turbulence models. The ParaView (Open source software) or other standard post-processing tools like Tecplot or Gnuplot can be used to post-process the results of OpenFOAM simulations [32].

2.7 Dimensional Analysis

Dimensional analysis provides a tool for simplifying and studying difficult physical problems. The concept of similarity is central to dimensional analysis. In physical terms, resemblance refers to some equivalence between two distinct entities or phenomena. Prior to beginning any study, it is critical to undertake a dimensional analysis to determine which factors should be investigated.

The dimensional analysis is carried out using the Buckingham π-Theorem. A dimensional problem with n variables can be reduced to a nondimensional problem with $m = n - r$ nondimensional terms. There are 10 study variables for baffle drop shaft that were considered for the dimensional analysis as follows:

- H – Total drop height
- Q – Discharge
- h – Baffle spacing
- B – Baffle width
- θ – Baffle rotating angle
- ρ – Density
- μ – Dynamic viscosity
- σ – surface tension
- g – Acceleration due to gravity

- η – efficiency of energy dissipation

The rate efficiency of energy dissipation can then be representated as a function of the dimensional variables as

$$\eta = \mathbf{f}(\mathbf{H}, \mathbf{Q}, \mathbf{h}, \mathbf{B}, \theta, \rho, \mu, \sigma, \mathbf{g}) \tag{2.4}$$

Given that all three basic dimensions in the problem, seven dimensionless groups can be obtained by considering Q, h and ρ as repeating (scaling) variables. Equations (2.5)-(2.11) show these nondimensional π groups.

$$\pi_{\mathbf{1}} = \mathbf{H}/\mathbf{h} \tag{2.5}$$

$$\pi_{\mathbf{2}} = \mathbf{B}/\mathbf{h} \tag{2.6}$$

$$\pi_{\mathbf{3}} = \theta \tag{2.7}$$

$$\pi_{\mathbf{4}} = \frac{\mathbf{Q}\rho}{\mu\mathbf{h}} = \frac{\mathbf{vh}}{\nu} = \mathbf{Re} \tag{2.8}$$

$$\pi_{\mathbf{5}} = \frac{\sigma\mathbf{h^3}}{\mathbf{Q^2}\rho} = \frac{\rho\mathbf{hv^2}}{\sigma} = \mathbf{We} \tag{2.9}$$

$$\pi_{\mathbf{6}} = \frac{\mathbf{Q^2}}{\mathbf{gh^5}} \tag{2.10}$$

$$\pi_{\mathbf{7}} = \eta \tag{2.11}$$

In the present study, both Reynolds number and Weber number will be sufficiently high (above the thresholds recommended earlier). Equation (2.4) can then be rearranged to obtain the final form of the efficiency of energy dissipation

$$\eta = \mathbf{f}(\mathbf{H/h}, \mathbf{B/h}, \theta, \frac{\mathbf{Q^2}}{\mathbf{gh^5}}). \tag{2.12}$$

Chapter 3

Physical Model Study

This research is carried out in two phases. The first phase was a physical model study that was conducted at the Asian Institute of Technology (AIT) in Thailand. The second phase is a computational model study conducted at Colorado State University (CSU). In this chapter, the methodology and results of the physical model are discussed. Physical modeling is a well-established approach for hydraulic research. It connects what can be correctly approximated using numerical models with the real world. It also makes numerical model calibration easier and boosts confidence in CFD model predictions. The scale of the physical model is one of the main criteria in physical modeling. The scale was selected based on Froude number similarity. Data acquired from physical model study will be used to validate the CFD model.

3.1 Model Scale selection

Generally the largest scale feasible for the available testing facility is chosen. The selection of scale may be influenced by restrictions other than the actual model's dimensions, for example available pumping capacity, available water storage capacity, and availability of materials. The baffle drop shaft model was constructed to a geometric scale (L_r) of 1:10 in the Water Engineering and Management (WEM) Hydraulics Laboratory at AIT. The Froude number similarity method is used because the dominant forces are gravity and inertia in the drop structure. The scale was selected to ensure that Re $> \mathbf{1x10^5}$ and $\mathbf{We} \geq \mathbf{32}$ for different discharge values. The initial model scale was selected to evaluate discharges higher than 25 l/s. The flow conditions were limited to free flow conditions in the baffle drop shaft. A 1:10 scale model scale was chosen which allowed a few cases with low Reynolds numbers $> \mathbf{1x10^5}$, but the higher model scale allowed for reduced scale effects. Calculated values of Re, Fr and We for the baffle drop shaft model are shown in Table 3.1 for shaft diameters of 0.9 m, baffle spacing of 0.28 m, and baffle rotating angle of $\mathbf{250}^\circ$ for discharges ranging from 8 l/s to 40 l/s of model scale.

Table 3.1: Fr, Re, We for baffle drop shaft physical model

Discharge (l/s)	Velocity (m/s)	Inlet Water Depth (m)	Fr	Re	We
8	0.397	0.065	0.50	30247	12.0
16	0.501	0.103	0.50	60493	19.1
24	0.600	0.129	0.53	90740	25.5
32	0.679	0.152	0.56	120987	31.4
40	0.746	0.173	0.57	151233	36.8

The prototype roughness of the concrete is 0.013 and transparent PVC plastic with a roughness of 0.009 was used in the physical model. Based on these results, the physical hydraulic model met the minimum requirements for Re and We for higher discharges. Thus, air entrainment in the model can fairly represent the air entrainment in the prototype given that there is less air entrainment at low flow conditions. The scale ratios used for different parameters in the physical model are listed in Table 3.2. The layout of the physical model of the baffle drop shaft is shown in Figure 3.1. The constructed physical model at WEM Hydraulics Lab is shown in Figure 3.2.

Table 3.2: Scale ratios used in physical model.

Parameter	Scale Relation	Scale Ratios
Length	$\mathbf{L_r = L_p/L_m}$	10
Velocity	$\mathbf{V_r = (L_r)^{1/2}}$	3.16
Discharge	$\mathbf{Q_r = (L_r)^{5/2}}$	316.23
Roughness	$\mathbf{n_r = (L_r)^{1/6}}$	1.48
Pressure head	$\mathbf{h_r = L_r}$	10

In contrast to the conventional design, which typically employs half of the shaft as the wet zone where the water flows, the study's baffle drop shaft design effectively utilizes the space in the shaft. Additionally, because it flows more slowly, air entrained bubbles can escape through the air windows as it moves through the shaft. Figure 3.3 illustrates how the baffle drop shaft's cross-section was designed.

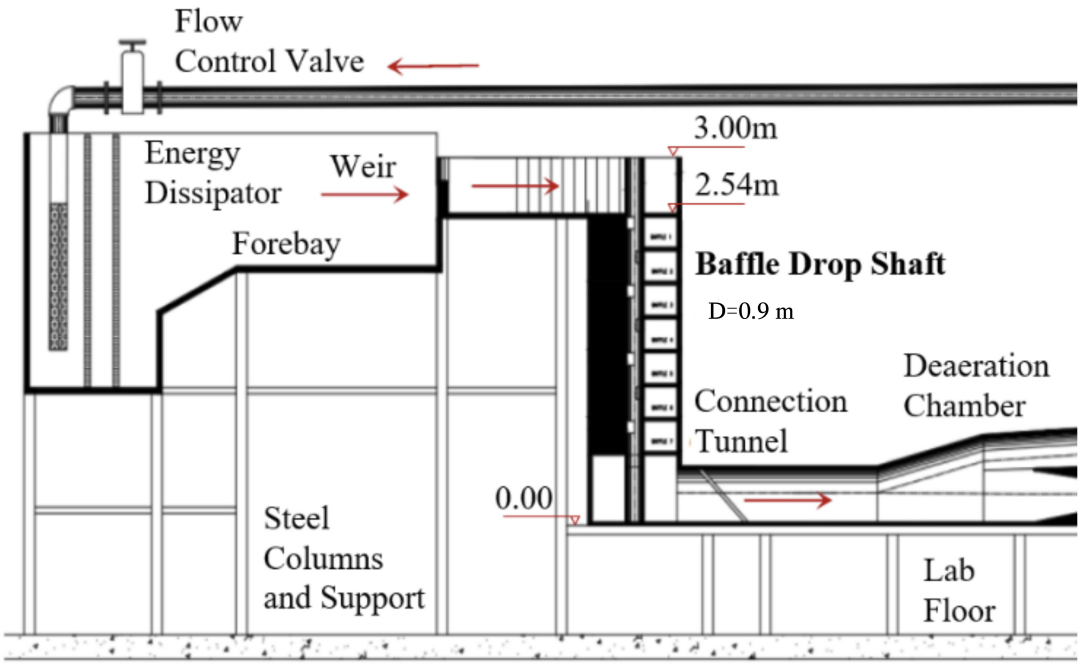

Figure 3.1: The layout of WEM baffle drop shaft

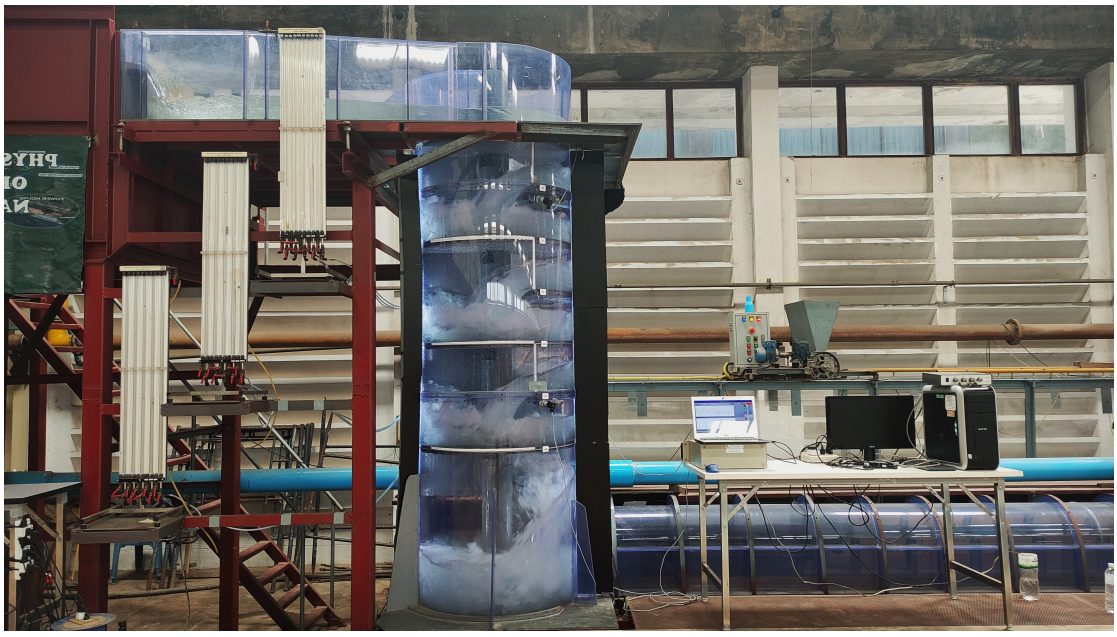

Figure 3.2: Constructed physical model

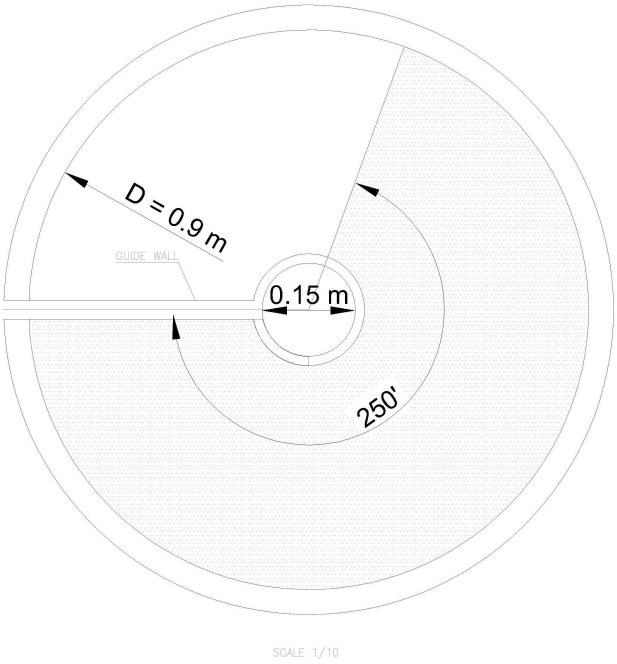

Figure 3.3: Baffle layout of the drop shaft

3.2 Experimental setup

After selecting the required scale of 1:10 that satisfies Froude number similarity, the model was constructed using PVC plastic with a roughness of 0.009. The outer shaft was constructed using transparent PVC plastic, and the baffle, inner shaft, and block wall were constructed using PVC plastic (see Figure 3.2 and 3.4). A Model with shaft diameters of 0.9 m, baffle spacing of 0.28 m, and baffle rotating angles of 250° was constructed. The inlet is tangential, with the approach flow rapidly diverging in the direction of the shaft before taking on the characteristic helicoidal configuration.

Even though the drop shaft and pumps can deliver 58 l/s discharge from a constant head tank, some trials were performed to identify the maximum discharge that could satisfy the free flow condition. The velocity measurement was done 3 cm above the baffle surface to avoid uncertainty due to the close surface; hence, the minimum discharge was set to 8 l/s. Approach flow was subcritical, and inlet velocity and water depth were also measured. Printed rulers were installed at

the edge of the baffle and along the block wall to measure the water depth inside the baffle drop shaft.

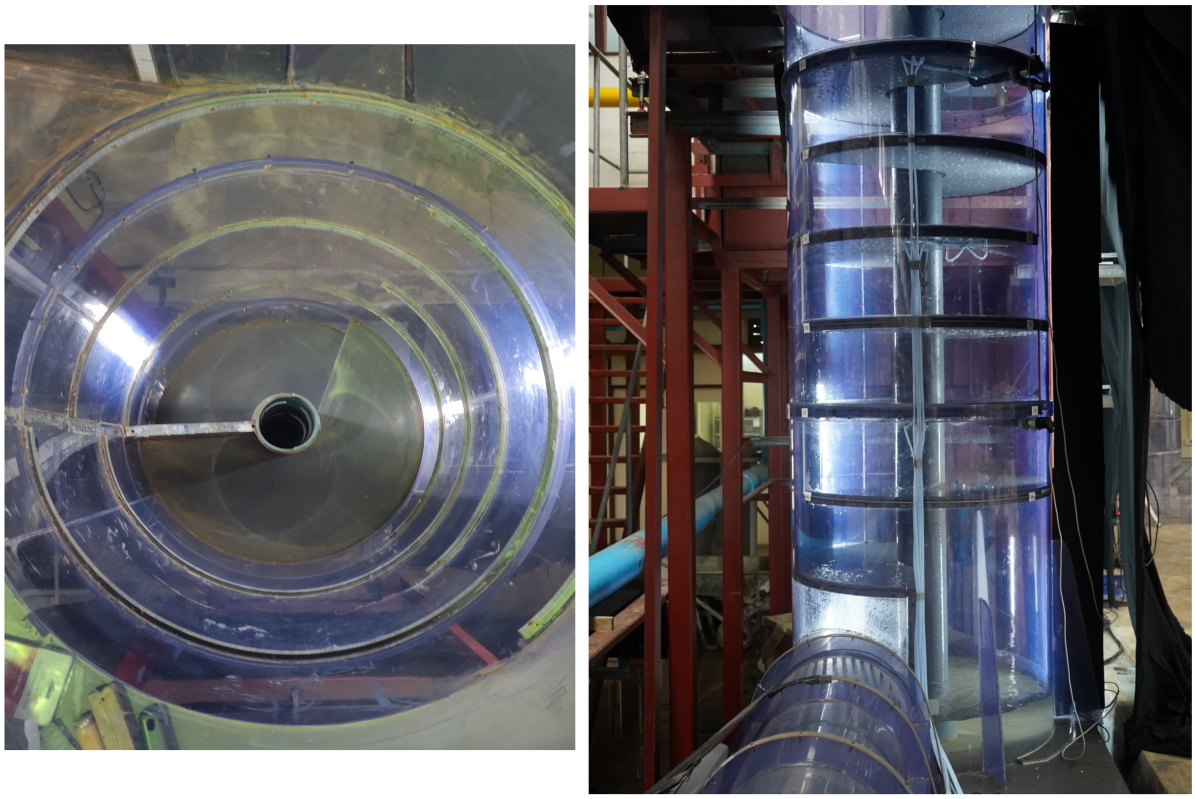

Figure 3.4: Material selection for different components of baffle drop shaft

3.2.1 Physical model configurations

Table 3.3 shows the five test configurations that were used in the physical model. These discharge values were determined by trial test runs using an existing novel baffle drop shaft to satisfy free flow conditions and laboratory limitations. Maximum baffle spacing according to the jet trajectory is 3.8m [7], hence baffle spacing is limited to 2.8 m at the prototype scale.

Table 3.3: Physical model configurations.

	Diameter(m)	(Baffle spacing (m)	Discharge (l/s)				
Prototype	9	2.5	2530	5060	7589	10119	12649
Model	0.9	0.28	8	16	24	32	40

3.3 Instrumentation

The main objective of the physical model study was to investigate the energy dissipation and identify the dynamics of the baffle drop shaft. While understanding the energetics and dynamics of the baffle drop shaft, pressure and velocity measurements can be used to validate the CFD model in the second part of the study. Experimental setups consist of pumps, approaches and existing conduits, flow-control valves, and a model of a baffle drop shaft. Apart from these setups, velocity and pressure measuring devices were installed at certain locations. The focus was to obtain experimental measurements of:

1. Approach discharge of the baffle drop shaft (Q)
2. Inlet and outlet water depths
3. Velocity measurement at inlet and on the baffles
4. Pressure measurement at edges of baffles
5. Water level measurement and water jet length on baffles

The discharge was measured with an electromagnetic flow meter. Inlet water depth was measured using a point gauge. Outlet water level was fluctuating; hence, recorded videos of the flow were used to obtain the average water level. Velocity and pressure measurements are described next.

3.3.1 Velocity measurements

Velocity was measured using an electromagnetic velocimeter at the inlet and at two locations (the center and near the outer shaft) on the first and fifth baffles (see Figure 3.5). Velocity measurements on baffles will be used to validate the CFD models. Electromagnetic flow meters are volumetric flow meters that measure fluid velocity using electromagnetic induction. When measuring water-based fluids, this method of measurement is highly accurate.

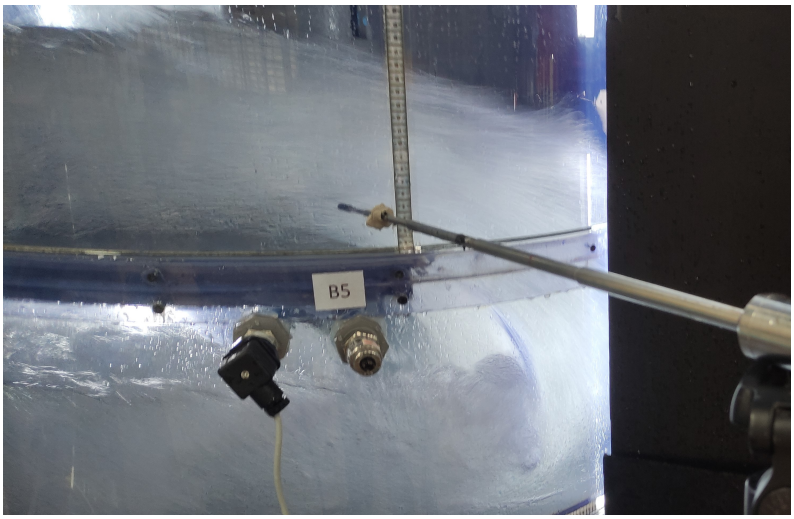

Figure 3.5: Velocity measurements in a model baffle drop shaft using electromagnetic flow meter

3.3.2 Pressure measurements

For the measurements of hydrodynamic pressures, Low Range Industrial Pressure Transmitters were installed at edge of the baffle 1 and baffle 5. The pressure sensors and data acquisition system have the following specifications.

- Pressure Range (mbar): 100 mBar
- Accuracy: (Thermal Zero Shift): <+/- 0.04 %
- Operating Temperature: -20 to 80^oC
- NI Card DAQ: 16 bits, 250 kS/s

Placing pressure sensors under the baffle is the most suitable location. Due to limited available resources and considering the safety of the pressure sensors, pressure sensors were installed outside the outer shaft using a bend pipe as shown Figure 3.6. The data acquisition system is shown in Figure 3.7

Figure 3.6: Pressure sensors installed under the baffle using separate bend pipe

Figure 3.7: Data Acquisition System

3.4 Results

3.4.1 Flow regime

The characteristics of the fluid and the geometry of the system together determine a flow regime, which is the pattern of fluid motion in a system. In the context of drop shafts, flow regimes are classified based on different inlet and outlet control conditions, which include free flow, pressurized outflow, and fully submerged baffle drop shaft conditions. The classification of flow regimes is important for designing baffle drop shafts that can effectively control water flow and prevent erosion and damage to downstream structures. Understanding the flow regime is also critical for predicting energy dissipation in baffle drop shafts under different conditions.

In the context of the experimental investigation of hydraulic characteristics and energy dissipation in a baffle-drop shaft, the main flow regime is free flow by design/restriction. Five different discharges provide different free flow conditions. Figure 3.8, Figure 3.9 and Figure 3.10 illustrate the flow regime from the front view, block wall view, and outlet channel view, respectively.

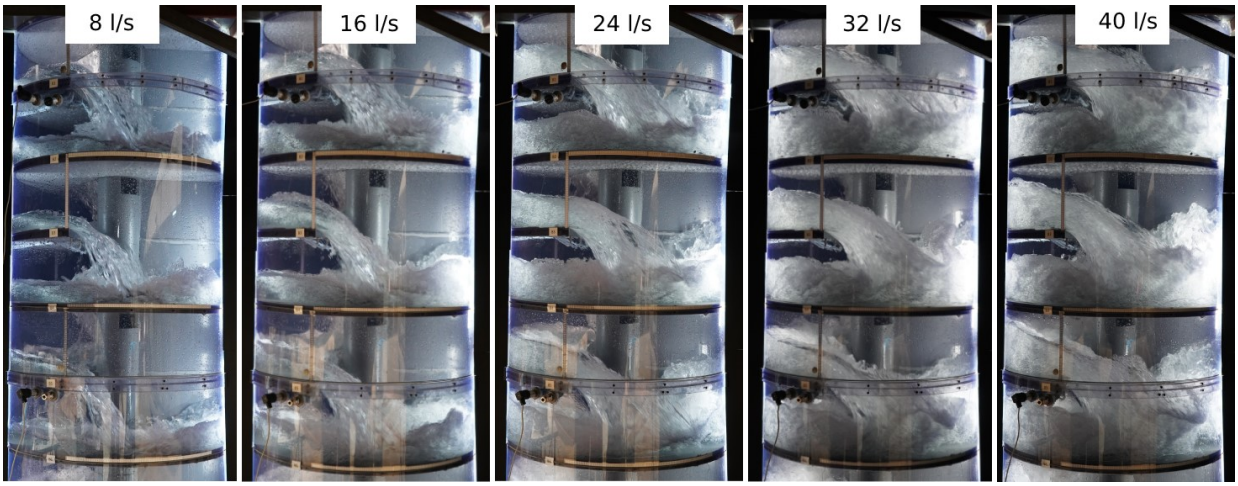

Figure 3.8: Water flow in physical model for different discharges - view from front side

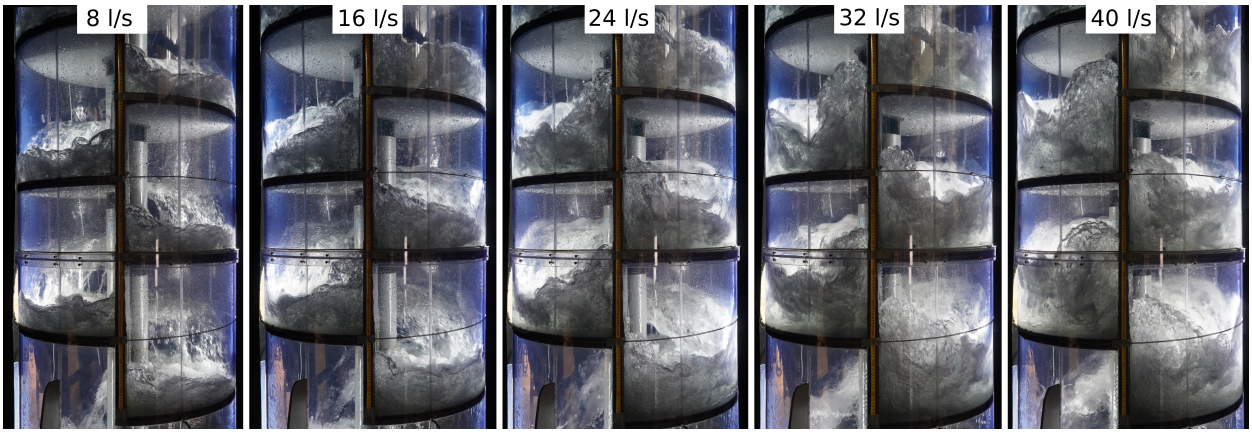

Figure 3.9: Water flow in physical model for different discharges - view from block wall

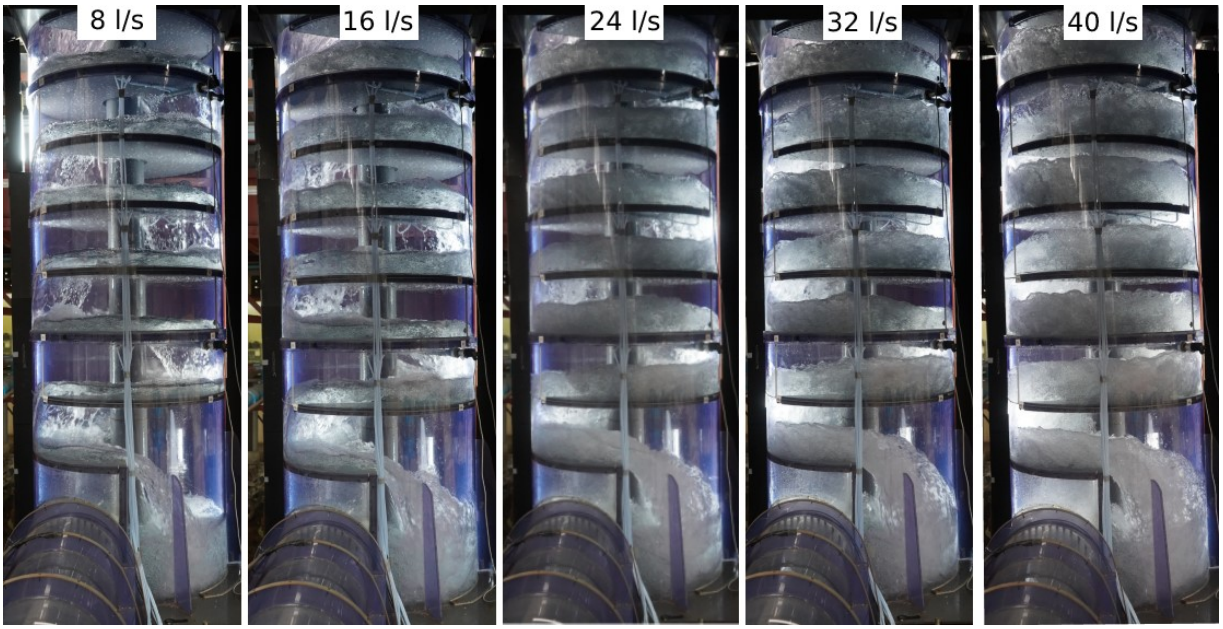

Figure 3.10: Water flow in physical model for different discharges - view from outlet

The water flows tangentially from the inlet channel into the drop shaft and from the drop shaft to the outlet channel. When water from the inlet channel entered the drop shaft, it impacted the first baffle. The water then began to flow down the drop shaft. Due to the inertia of the water and the obstruction of the block wall and baffles, the velocity of the water was redistributed along the baffles. Some of the water jetted into the lower baffle along the outer shaft of the baffle as jet flow, but for the lowest flow rate (8 l/s), nappe flow occurred. The block wall acts as a major disruptor of the inertia in the flow creating fully turbulent flow conditions and rolling waves on baffles. Rolling waves and jets that came from the baffle above increased the turbulence in the flow that gets propagated to the baffle edge. Water cascades repetitively and impacts the water condensation on the lower baffle as it rolls between the baffle and shaft wall. The impact wave exhibited impingement, friction, aeration, fragmentation, and coalescence, resulting in increased flow resistance and energy loss. Thus, the impact flow on the baffle was one of the primary energy dissipation mechanisms in the drop shaft. When the water reached the bottom of the drop shaft, it collided with the lower water and merged with the water that had been reflected. The final form of energy loss from the drop shaft was impingement and the high turbulent conditions of the flow.

The flow is aerated because the free surfaces interact with the air above and below the nappe and because the nappe contacts and sputters against the baffle. These interactions cause the water's surface to break up into droplets and generate turbulence, thereby entraining atmospheric air. On the unrestricted surface, the splashing, mixing, and churning actions promote air entrainment. Due to cascading and high turbulent conditions, significant air entrainment occurs. The formation of bubbles and the incorporation of air into water result from the free fall of water from baffles cascades and its subsequent mixing with the surrounding air. Air entrainment can aid in decreasing water velocity and dissipating energy, thereby preventing erosion and damage to downstream infrastructure. However, excessive air entrainment can lead to issues such as decreased efficacy and increased maintenance needs for downstream equipment in hydropower plants. Therefore, it is essential to design hydraulic structures meticulously to optimize air entrainment for their intended function.

Based on visual observation, the flow regime in all the baffles appear to be quite similar. Average water depths and jet lengths were measured using installed rulers at the edge of the baffle and along the block wall. Using image analysis and linear measurements, flow regimes seem to be repetitive from baffle to baffle.

Table 3.4: Measured average water depth at edge of the baffle (h_1), average jet length from edge of the baffle (L) and average maximum water level near the block wall (h_2) for each and every baffle

.

Discharge (l/s)	h_1 (cm)	L (cm)	h_2 (cm)
8	5.2 ± 0.3	29.2 ±1	18.0 ± 0.4
16	8.5 ± 0.4	41.0 ±0.8	25.8 ± 0.1
24	10.6 ± 0.4	45.2 ±0.6	34.2 ± 0.3
32	12.3 ± 0.3	51.2 ±0.6	39.1 ± 0.6
40	14.7 ± 0.3	59.0 ±0.5	41.2 ± 0.2

3.4.2 Pressure

Four pressure measurements were collected at two locations for baffle 1 and baffle 5 for all 5 discharges at the baffle edge. One location was the center of the baffle edge, and the other was 5 cm away from the outer shaft. Figure 3.11 show the time-averaged pressure distribution in the middle and corner for a discharge of 24 l/s.

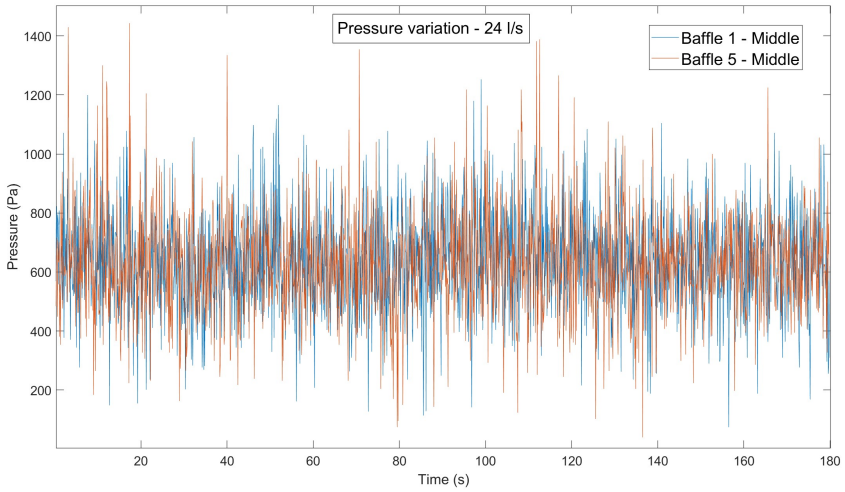

(a)

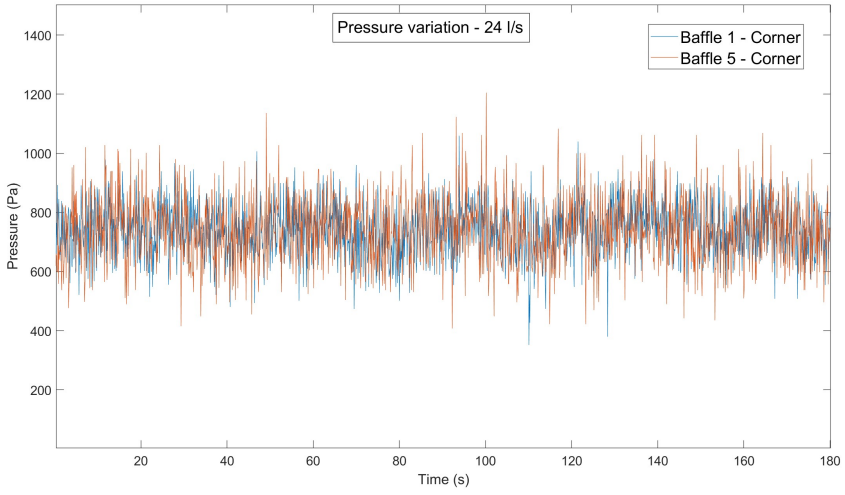

(b)

Figure 3.11: Pressure measurements as a function of time at a discharge of 24 l/s: (a) at the center of baffle; (b) at the edge of baffle.

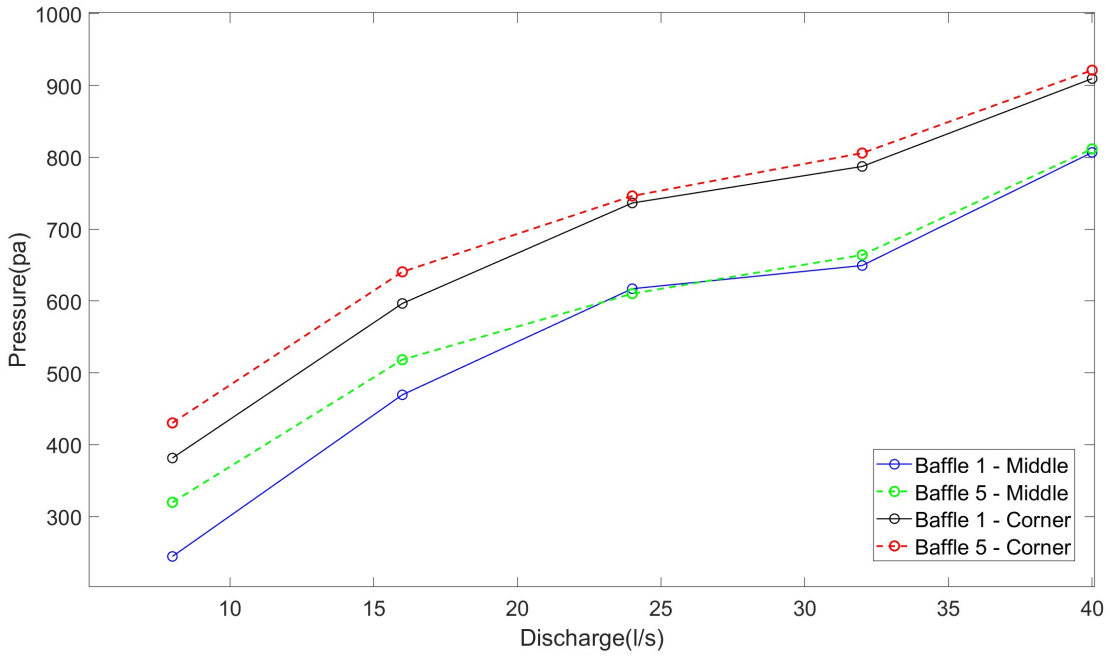

Figure 3.12: Pressure measurements on baffle edge versus discharge

Figure 3.12 illustrates the average pressure distribution with respect to discharge at four pressure sensor locations. Water cascades between staggered baffles, but due to the asymmetric impact of the flow, pressure distribution on the baffle varies with the orientation of the baffle. The maximum pressure on a given baffle is not the main focus of the physical model study. The pressure measurements at the baffle edge indicates that a similar (repetitive) low regime occurs at each and every baffle. The average pressure increases with the discharge as shown in Figure 3.12.

Baffles are the most vulnerable structural element of the baffle drop shaft because they need to withstand against the impact of the water jet, the weight of the water cushion, and self weight. Thus, there is a need to determine the maximum pressure on the baffle. However, determining the maximum pressure experimentally using pressure sensors is difficult due to cost and logistical challenges associated with installation. A primary use of these pressure measurements is for validation of the CFD model.

3.4.3 Velocity

Velocity was measured in the same locations on the baffle as pressure measurements, but 30 mm above the baffle surface. Figure 3.13 shows velocity versus discharge from the physical model study. Velocity measurements at the inlet and outlet of the shaft were also made to calculate the global energy dissipation. Measured velocity on baffles increases with discharge, but velocity values are slightly different (less than 9% difference) on the two baffles. Table 3.5 summarizes the average inlet and outlet velocities of each discharge. Inlet velocity was measured using the electromagnetic velocity meter, and outlet velocity was calculated using the measured cross sectional area of the outlet conveyance.

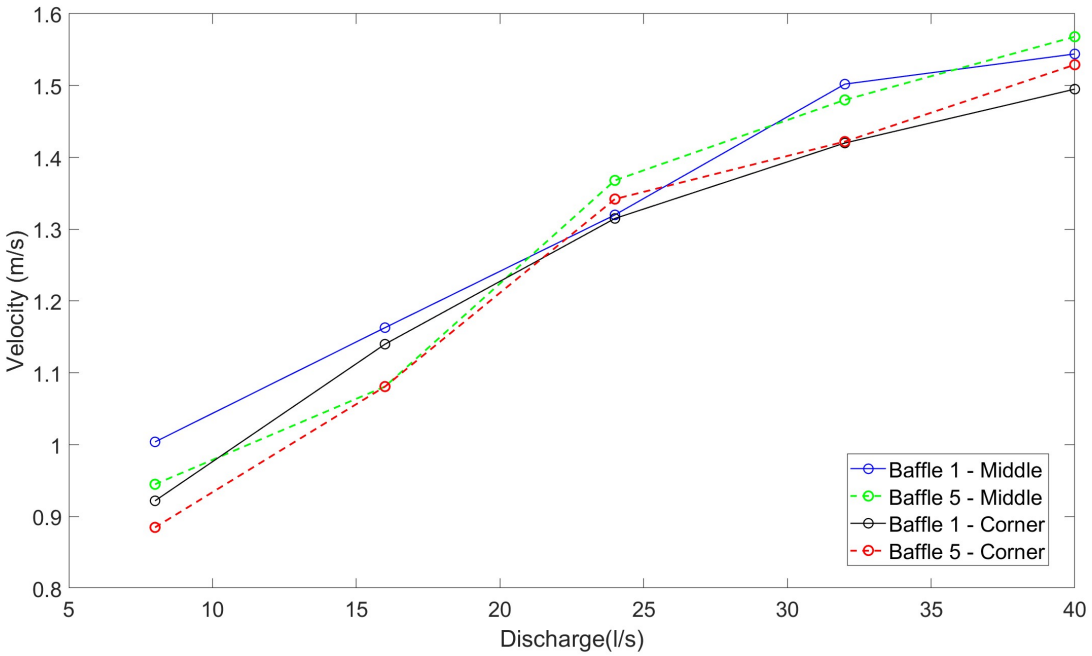

Figure 3.13: Velocity measurements at baffle edge versus discharge

Table 3.5: Inlet and outlet velocity of the baffle drop shaft for different discharges

Discharge (l/s)	Inlet velocity (m/s)	Outlet velocity (m/s)
8	0.40	0.09
16	0.50	0.15
24	0.62	0.21
32	0.68	0.27
40	0.75	0.33

3.4.4 Energy dissipation

The potential energy of fluid flow is converted into other forms of energy, such as kinetic energy and internal energy, etc. Flow conditions in the baffle drop shaft were highly turbulent, with both the inlet and outlet channels under open channel flow. The 2.57 m elevation difference was divided by seven staggered baffles. Mainly energy loss occurs due to the following causes

- The impact of the falling flow on the baffle
- Complex flow pattern due to turbulence
- Friction on the baffle and outer shaft
- High air entrainment

The superposition of the above dissipation mechanisms creates a good energy dissipator. To quantify the efficiency of energy dissipation η, global energy dissipation was defined as follows using total available energy head ((4.1)at inlet and outlet,

$$\mathbf{E} = \mathbf{z} + \frac{\mathbf{P}}{\rho \mathbf{g}} + \frac{\mathbf{v^2}}{\mathbf{2g}}, \tag{3.1}$$

where,

z = Elevation head

$\frac{P}{\rho g}$ = Pressure head

$\frac{v^2}{2g}$ = Velocity head

$$\eta = \frac{E_{in} - E_{out}}{E_{in}} \times 100\%, \tag{3.2}$$

where,

η = Efficiency of energy dissipation

E_{in} = Inlet channel total energy head

E_{out} = Outlet channel total energy head

A non dimensional discharge (Q^*) can be defined as follows

$$\mathbf{Q}^* = \frac{Q}{\sqrt{gH^5}}, \tag{3.3}$$

Where,

Q = Discharge

H = Total head (2.57 m)

g = Acceleration due to gravity (9.81 m/s)

The efficency of energy dissipation versus Q^* is shown in Figure 3.14

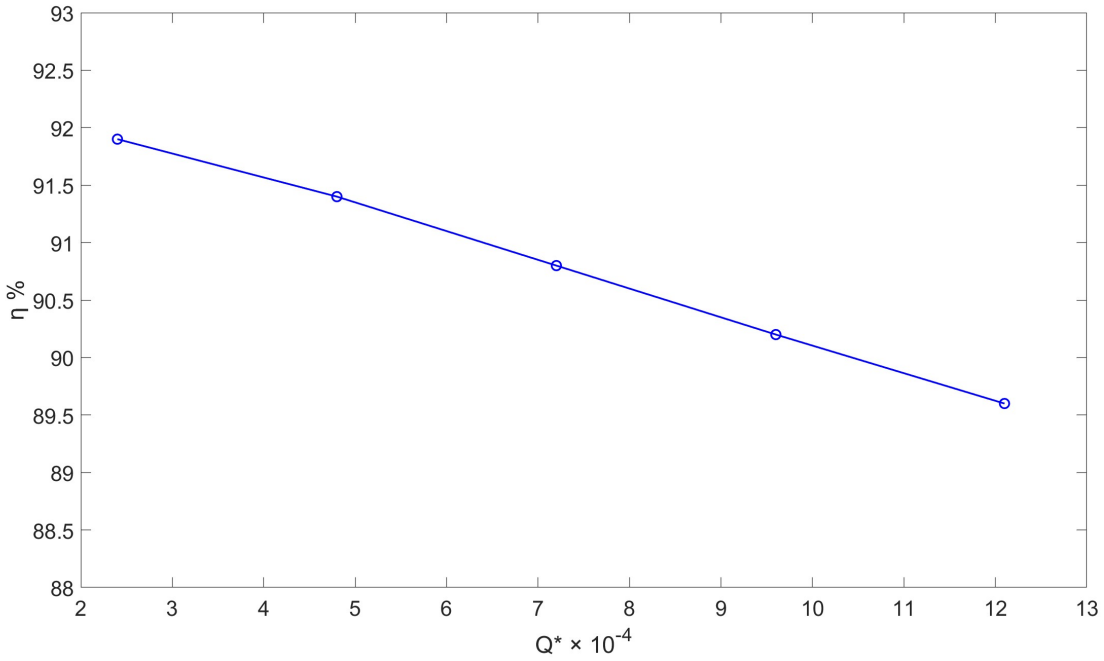

Figure 3.14: Efficiency of energy dissipation (η) of baffle drop shaft for different flow rates

It is clear that η decreases slightly with increase in Q* but remains at a high level. η varies from 91.9% to 89.6% under free flow conditions, indicating that baffle drop shafts are excellent energy dissipators from a global perspective. This evidence is consistent with previous physical observations of various drop shafts. By altering Q*, tall drop shafts do not generate a significant change in energy head loss.

Chapter 4

Computational Model Study

The physical model study was conducted using only five configurations which is not sufficient to perform a detailed parametric study. CFD is a viable option for an indepth investigation of the energetics and dynamics of the baffle drop shaft. In this chapter of the thesis, a broader range of configurations will be investigated using CFD.

4.1 Numerical Model

The CFD models have been built to simulate the hydraulic behavior of baffle drop shaft using OpenFoam. For the numerical solution of partial differential equations driving fluid flow and associated processes, OpenFOAM offers a variety of useful tools and solvers. The governing equations are discretized and solved on a mesh using the finite volume method. The software is adaptable for modeling diverse flow conditions since it incorporates a large variety of models and numerical techniques. According to the literature review, a suitable turbulence closure scheme to develop a CFD model for the present study is the RANS based realizable k – ϵ model. The following characteristics set the realizable k-ϵ model apart from the traditional k- ϵ model:

1. To satisfy some mathematical restrictions on the Reynolds stresses that are consistent with the physics of turbulent flows, a variable Cμ is incorporated into the turbulent viscosity formula.

2. Based on the dynamic equation of the mean-square vorticity fluctuation, a novel equation for dissipation is provided, in which neither the production term nor the destruction term have any singularities and the production term does not entail the production of k

In general, when the flow features involve severe streamline curvature, vortices, and rotation, the realizable k- ϵ model exhibits significant gains over the regular k- ϵ model [26].

4.1.1 Geometry

The 3D geometry of the prototype was constructed using Rhinoceros 3D, which is computer graphics and computer-aided design application software. Figure 4.1 illustrates the geometry of the novel baffle drop shaft. This 3D drawing must be watertight to satisfy continuity; otherwise, it will create errors in the model. The benchmark geometry with a height is 3.3 m, a shaft diameter of 0.9 m with baffle spacing of 0.28 m and a 270-degree baffle rotating angle. This initial model was used for validation. Geometry is fed to the CFD model as a stereolithography (STL) file. A total 10 geometric configurations were used in the parametric study as listed in Table 4.1.

Table 4.1: Geometric configurations for CFD parametric study

Shaft diameter, D (m)	Baffle spacing, h (m)	Baffle angle, θ
0.8	0.28	250
0.9	0.23	250
	0.28	180
		250
		270
	0.33	250
	0.38	250
	0.43	250
	0.48	250
1	0.28	250

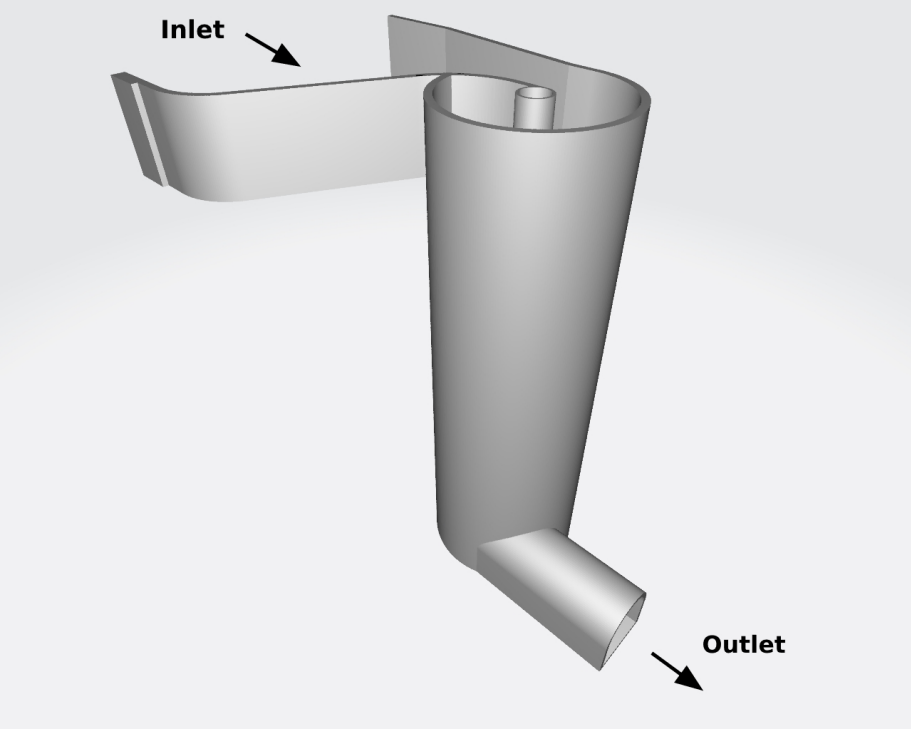

Figure 4.1: Benchmark geometry of the baffle drop shaft

4.1.2 Meshing

Meshing is one of the most important steps in CFD modeling. Meshing provides a discretized representation of the geometry of the problem domain. It divides the complex geometry into a number of smaller, simpler pieces (such as triangles, quadrilaterals, tetrahedra, or hexahedra) that the numerical solution techniques used in CFD simulations can handle. The quality of the mesh affects the precision and dependability of CFD simulations. The flow dynamics and gradients inside the domain can be accurately captured by a well-designed mesh with the right resolution and element form. In order to capture flow features in regions of interest with higher resolution, meshing enables local refinement and adaptation. The accuracy and effectiveness of the simulation can be increased by using adaptive mesh refinement techniques, which dynamically alter the mesh based on the flow solution to concentrate computational resources where they are most needed. The meshing of the domain in this study was constructed using openFoam's mesh generation utilities. They are blockMesh and snappyHexMesh.

The blockMesh utility creates parametric meshes with grading and curved edges. The mesh is generated from a dictionary file named blockMeshDict located in the constant/polyMesh directory of a case. The blockMesh reads this dictionary, generates the mesh and writes out the mesh data to points and faces, cells and boundary files in the same directory.

The snappyHexMesh utility generates 3-dimensional meshes containing hexahedra (hex) and split-hexahedra (split-hex) automatically from triangulated surface geometries in Stereolithography (STL) format. Cell splitting is performed according to the specification supplied by the user in the castellatedMeshControls sub-dictionary in the snappyHexMeshDict. Cell removal requires one or more regions enclosed entirely by a bounding surface within the domain. Final stage of meshing is moving cell vertex points onto surface geometry to remove the jagged castellated surface from the mesh. An example computational mesh is shown in Figure 4.2

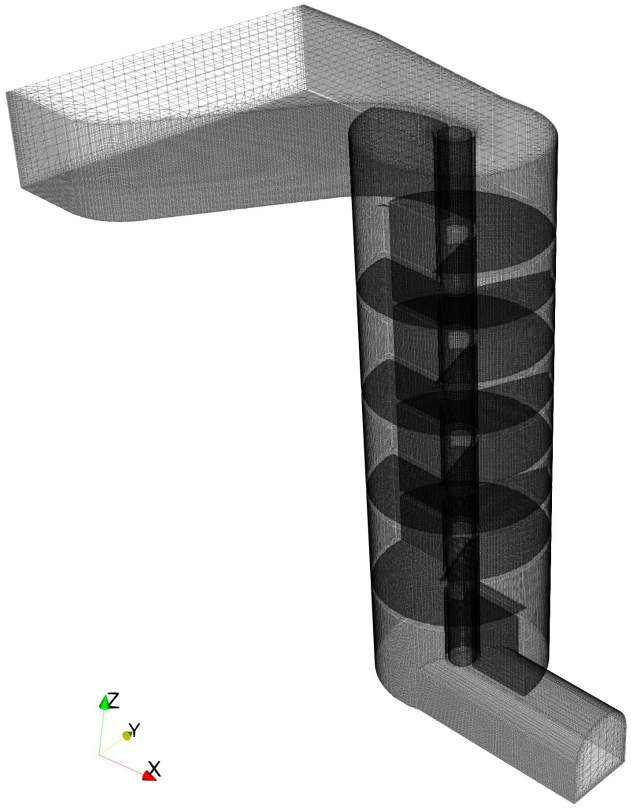

Figure 4.2: An example computational mesh of the baffle drop shaft

4.1.3 Multi-phase Solver

Identifying the water air interface is very important in free-surface flow studies such as this study because it helps in understanding and optimizing the performance of the baffle drop shaft with sufficient numerical accuracy. The position of the water surface can be tracked in the computational domain using the Volume of Fluid (VOF) model. VOF based multiphase model of InterFoam was used here to identify a sharp and well-defined interface. InterFOAM is expressly designed to solve two-phase flow problems, which it does by solving the continuity and momentum equations for each phase separately and tracking the interface between the two fluids. The solver employs the VOF algorithm to capture the motion and deformation of the interface between two fluids. Until convergence is achieved, the InterFOAM algorithm alternates between solving the momentum equations and revising the interface location using the VOF method. This enables simulation of fluid flow and monitoring of the interface between the two phases.

4.1.4 Grid independence analysis

A precise gridding exercise is the key to solving CFD. A number of grids with different mesh sizes are generated for the geometry in question, CFD calculations are run, and the change in results with each grid level is examined. This test's objective is to assess how grid resolution affects how accurate the results are. The numerical solution is grid independent if it mostly stays the same or converges to a consistent solution when the grid is refined. Usually, this sensitivity analysis is performed using only one point. Considering the high turbulence condition and the available data for velocity and pressure for the physical model study, four velocity locations (the exact location of the velocity measured in the physical model) and two pressure sensor locations were considered for this analysis. The numbers of cells for the different meshes for the grid independence study were 276,377, 556,775, 1,199,051, and 2,178,815, respectively.

According to the Figure 4.3, velocity converged even with 500,000 cells, but two pressure points did not. This implies that that the grid resolution is insufficient and that a more refined mesh is needed for converged solutions. A mesh with about 1.2 million cells resulted in convergence of

both the velocity and pressure values to a satisfactory level. Considering the computational cost, the 1.2 million-cell configuration was taken to be suitable for the parametric study.

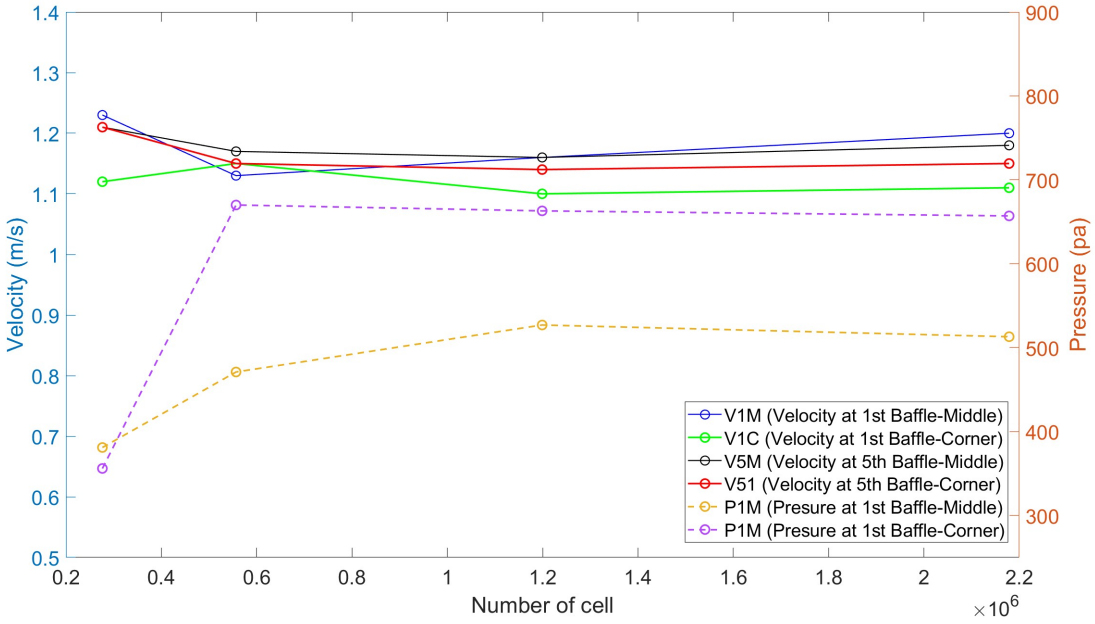

Figure 4.3: Results of grid independence

4.1.5 Model validation

Validation facilitates establishing the validity and applicability of the CFD model for a particular problem. It demonstrates that the model can predict physical phenomena precisely and provides a solid foundation for making decisions. The measurements at the four sensor locations in the physical model discussed in Chapter 3 were used to validate the CFD model. The velocity and pressure measurements from the physical model are compared with those from the CFD model as shown in Figures 4.4 and 4.5. Four velocity and four pressure measurements taken at a discharge of 24 l/s in the physical model with an outer shaft diameter of 0.9 m, baffle spacing of 0.28 m, and baffle rotating angle = 250^0).

Figure 4.4 shows that the average velocity of the CFD model converges to the experimental mean with a 4% to 10% relative error. Pressure variations at relevant locations are shown in

Figure 4.5. The relative error percentage between CFD and the physical model was around 9% to 15%. The time-averaged pressure values of the CFD model are always lower than the experimental pressure values. This may be due to the experimental error because the pressure sensor diaphragm may oscillate due to high fluctuations in the water surface in the baffle drop shaft. Overall, the numerical results and the experimental measurements are in good agreement providing confidence for using the CFD model for a detailed parametric study.

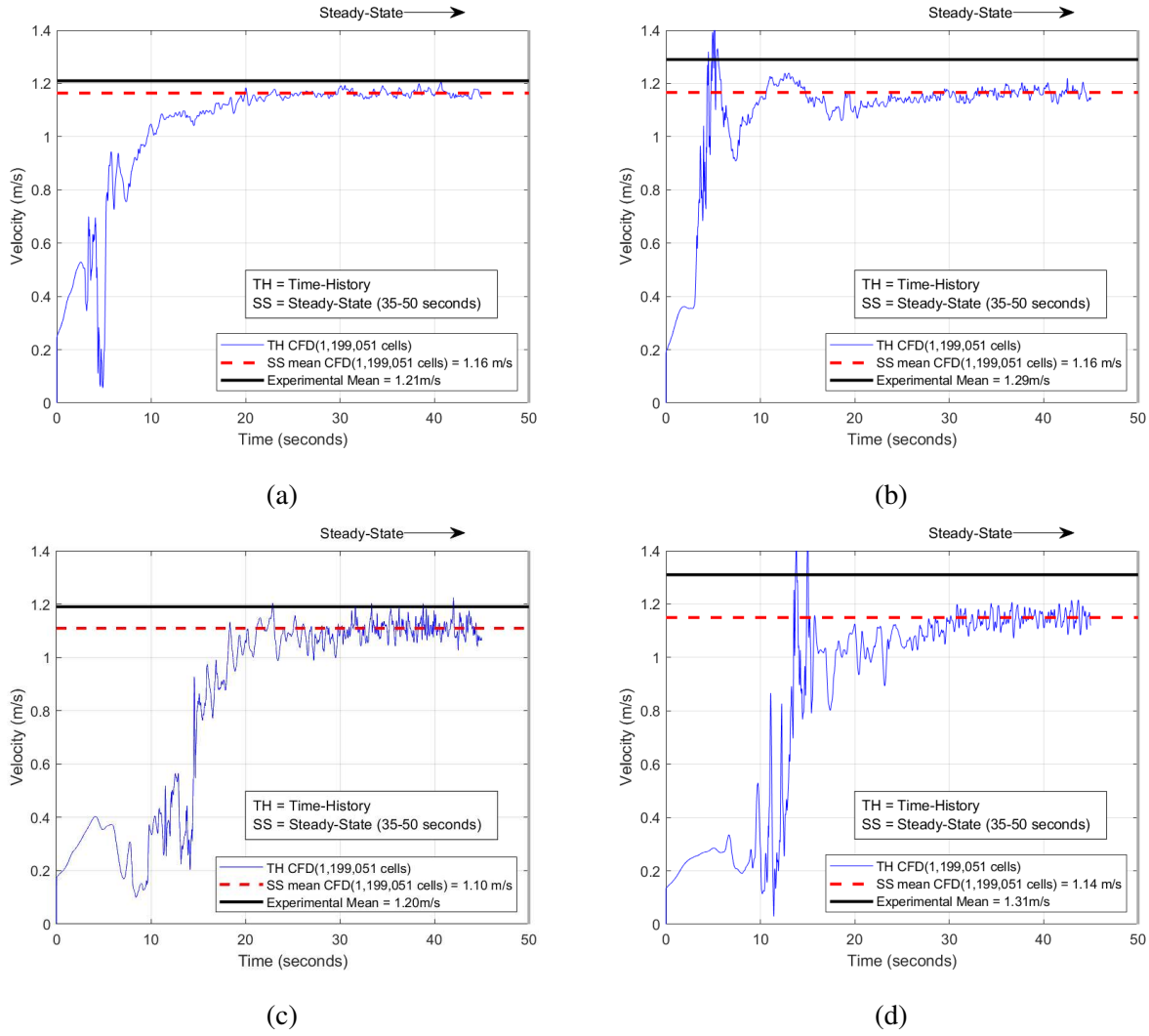

Figure 4.4: Model validation using velocity (m/s) on the baffle edge for 24 l/s: (a) First baffle - Middle (V1M) (b) First baffle - Corner (V1C) (c) Fifth baffle - Middle (V5M) (d) Fifth baffle - Corner (V5C)

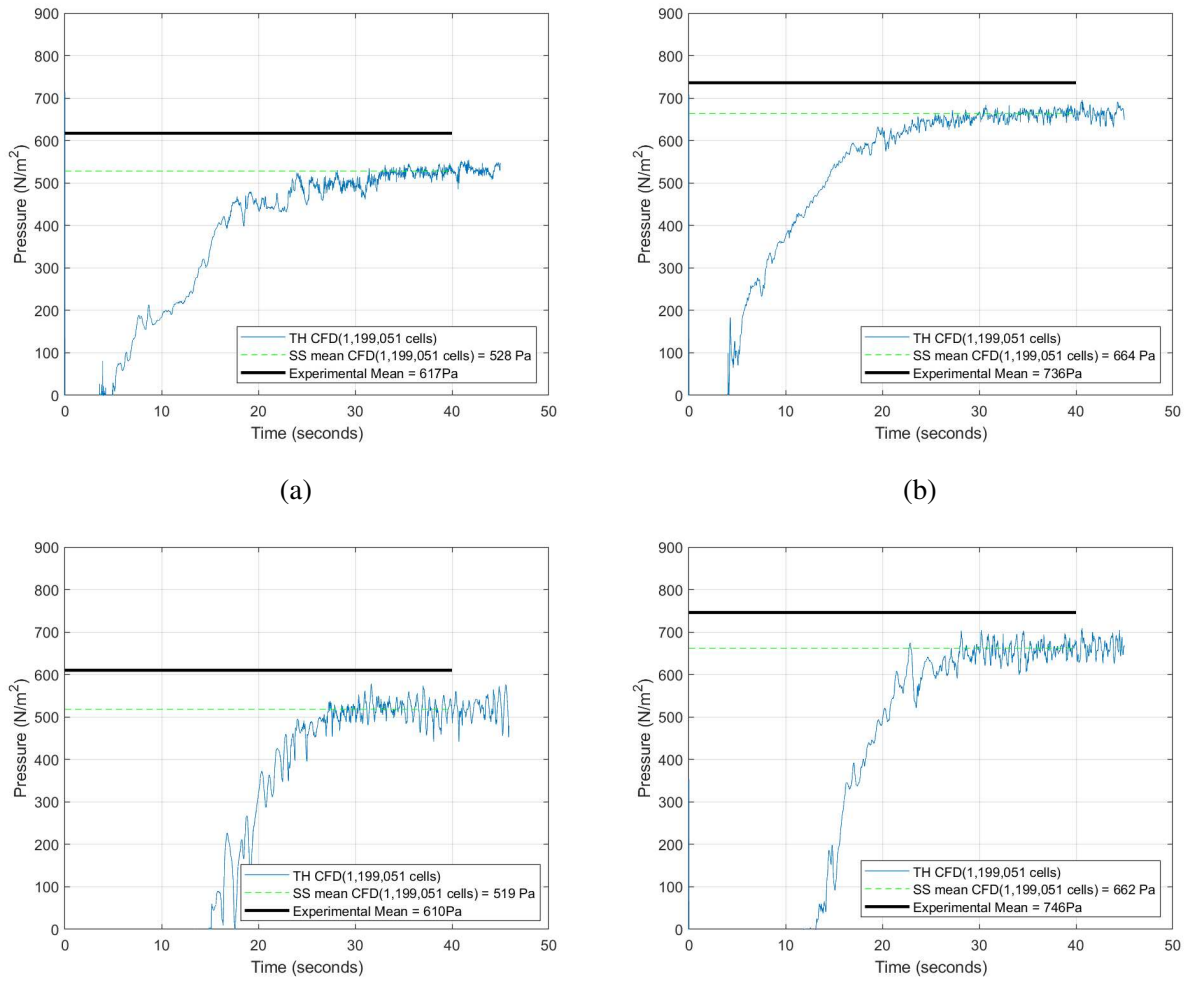

Figure 4.5: Model validation using pressure (Pa) on the baffle edge for 24 l/s: (a) First baffle - Middle (P1M); (b) First baffle - Corner (P1C); (c) Fifth baffle - Middle (P5M); (d) Fifth baffle - Corner (P5C).

4.1.6 Water profile validation

Water profile validation was done using images obtained from the physical model experiments at a discharge of 24 l/s. Comparing a physical model with a RANS model involves some limitations; mainly, physical model images provide instantaneous photos, but a CFD model provides the average condition of the flow. RANS CFD models rely on a variety of assumptions and simplifications to make mathematical calculations possible. These can include turbulence models and boundary conditions. In contrast, a general image comparison can be performed to identify if

there is any significant variation between the two models even though velocity and pressure values converged within the expected error margin. It seems that adding baffles to a simple plunge drop shaft increases the energy dissipation slightly due to friction of the baffles and shaft wall. Figures 4.6 and 4.7 show comparisons of water profiles at 8 l/s and 40 l/s between the experimental and numerical studies, respectively. It is evident that there is good overall qualitative agreement.

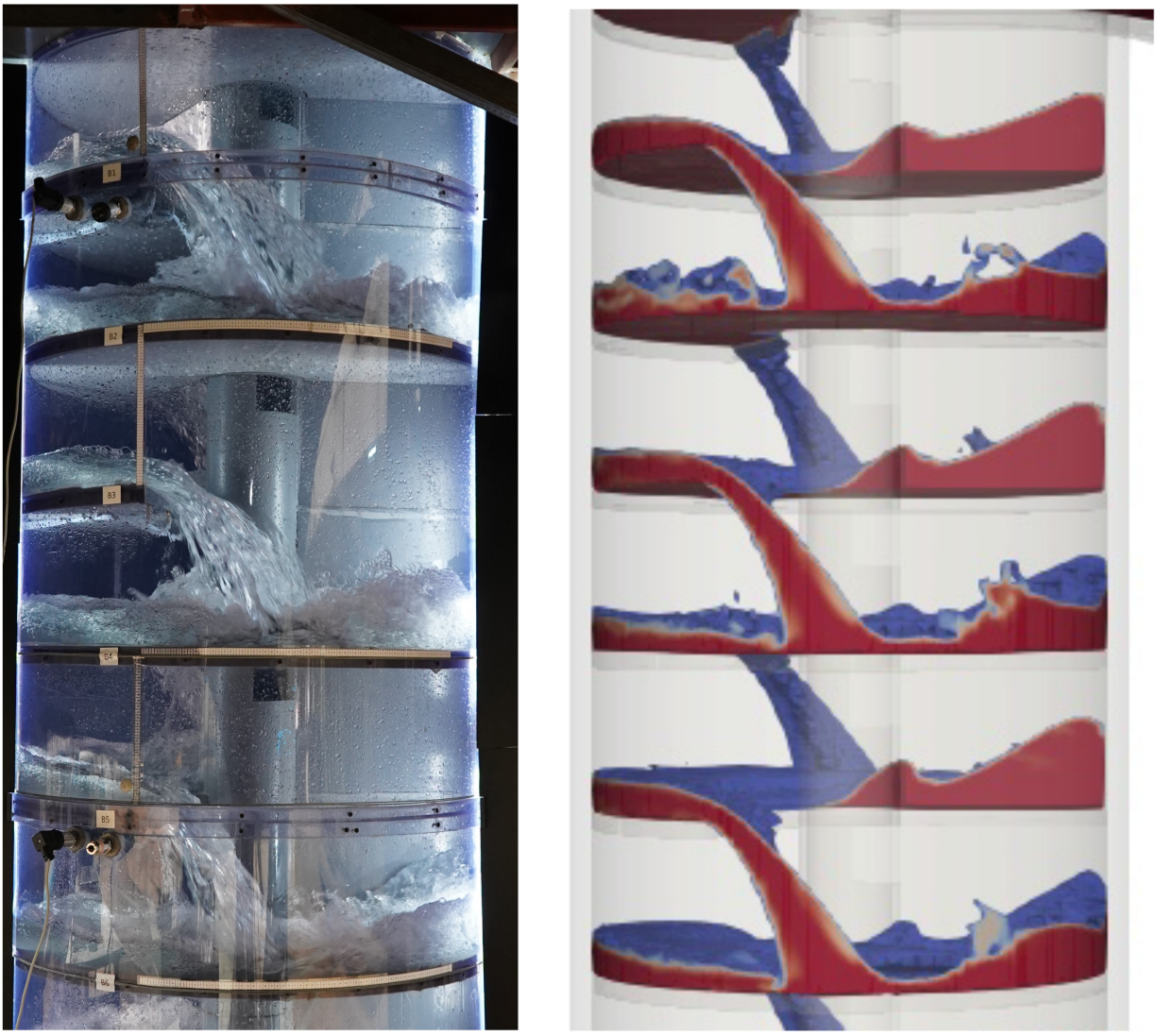

Figure 4.6: Water profile comparison - 8 l/s

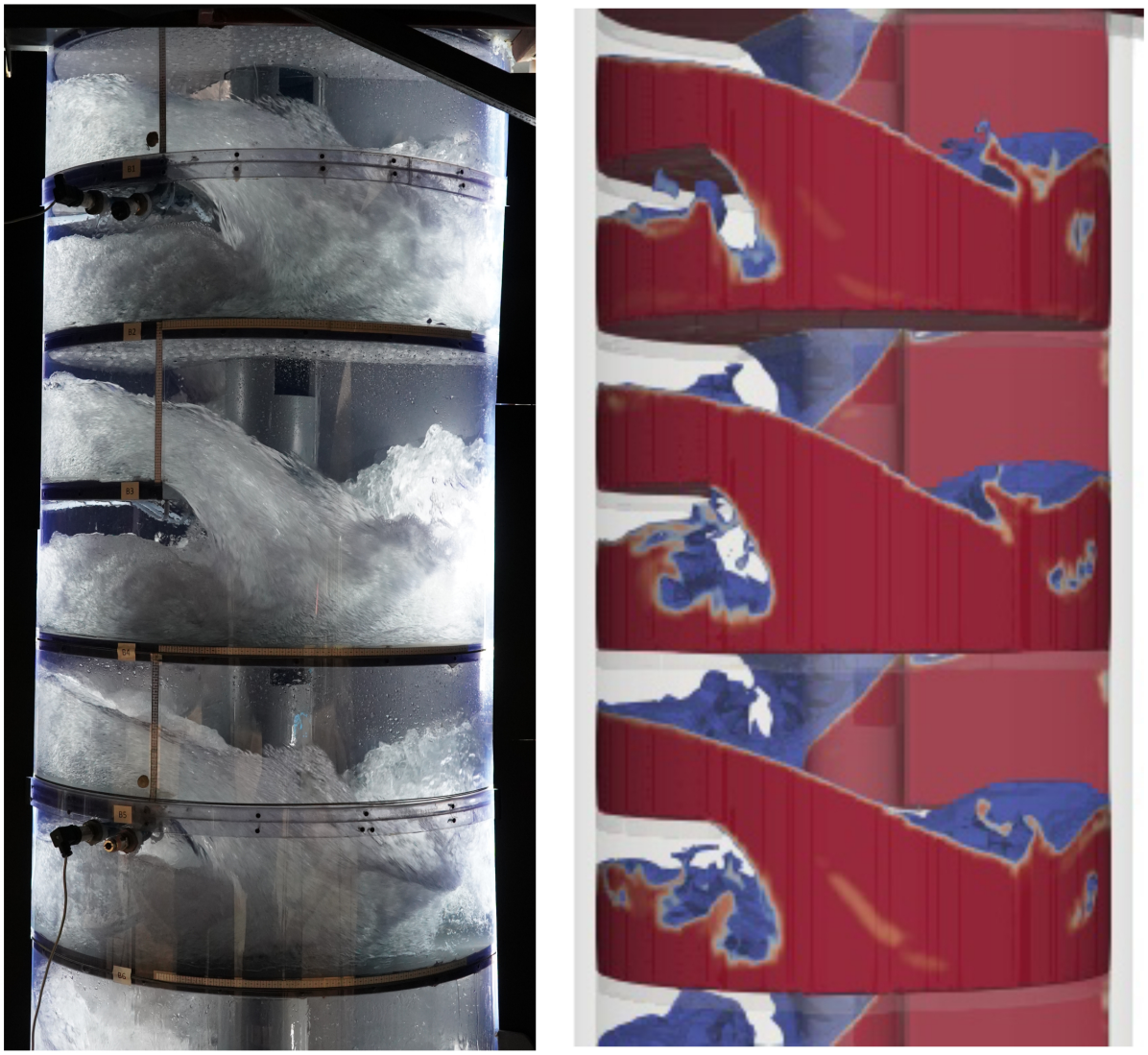

Figure 4.7: Water profile comparison - 40 l/s

4.1.7 Tracking the water surface

A phase fraction variable α must be defined because the volume fraction of the gas-liquid phase is added to capture the interface. A value of α = 1 indicates that the cell is full of water in the water-air mesh system. The volume of the flow increased due to high air entrainment in the baffle drop shaft resulting in bulking of the flow. Since there can be only two volume fractions, 0 and 1, shown in all grids, a large number of cells is required to trace the exact surface of the flow with air entrainment. However, using a large number of cells requires a high performance computer with a

higher computational cost. This study was developed based on the RANS model with the optimum number of cells; hence, it's unavoidable to get volume fractions between 0 and 1. There is a need to find an alpha value that satisfies air entrainment and water surface with the minimum error with respect to the physical model study.

To determine a reliable water surface, a plot the alpha valued across a line near a block wall is done as shown in Figure 4.8. The plot also show a side by side visual comparison between a snapshot of the flow in the experiment and the CFD simulation at the same time.

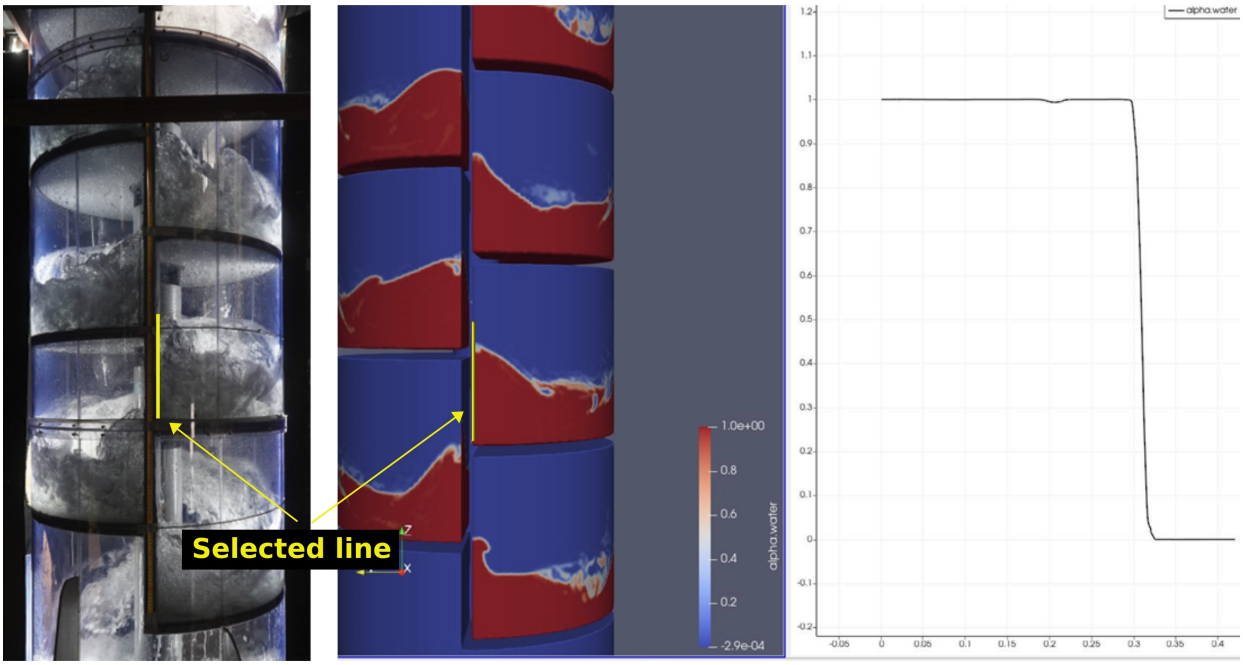

Figure 4.8: Alpha value change along a line

There is a clear difference near the wall surface. Measured averaged water depth along that line is 290 mm and the α value also changes around that depth. As a conservative estimate, an value of $\alpha = 0.5$ was considered as the a suitable threshold to determine the water surfaces in the simulations performed in this study.

4.2 Parametric study

CFD is a feasible tool for performing parametric studies because it provides the flexibility and ease to explore different design parameters such as shaft diameter, baffle spacing, and baffle rotating angle, in a cost effective manner. The Type 2 baffle drop shaft model was calibrated and convincingly validated using physical model results. The purpose of this parametric study is to gain insights into the energetics and dynamics through a baffle drop shaft and lay a solid foundation for further investigation of type two baffle drop shafts. We hypothesized that a baffle drop shaft is an effective energy dissipator and found this to be true from the experimental studies. However, there are other considerations that must be taken into account such air entrainment and pressure distributions on the baffle that critical for effective design.

In order to investigate these important parameters, a total of 27 configurations were simulated using three different shaft diameters, six baffle different spacing, and three baffle rotating angles, and one base case without baffles. Details of these configurations are presented in Table 4.2. The findings of the simulation were used to evaluate the influence of several factors, including discharge, energy dissipation, bulking, and pressure magnitudes. The goal is to gain some insights and provide guidance on how to choose the appropriate baffle spacing and optimize the structure for the implementation of this type 2 baffle drop shaft in storm water management system, hydropower, and treatment plants.

Table 4.2: Model configurations for the parametric study

Shaft diameter, D (m)	Baffle spacing, h (m)	Baffle angle, θ	Discharge (l/s)
0.8	0.28	250	8, 24, 40
0.9	0.23	250	8, 24, 40
	0.28	180	8, 24, 40
		250	8, 16, 24, 32, 40
		270	8, 24, 40
	0.33	250	8, 24. 40
	0.38	250	40
	0.43	250	40
	0.48	250	40
1	0.28	250	40
0.9	No baffles		40

4.3 Energy dissipation

4.3.1 Global energy dissipation

After computing the total energy loss, which is the difference in the total energy between two designated measurement locations, namely the entrance and the exit of the model depicted in Figure 4.1 , the efficiency of energy dissipation η was calculated. This difference can be thought of as the difference between the two total energies. Elevation, pressure, and velocity heads were all added up to get the total energy at both of these locations. To perform this task, as shown in Figure 4.9, each and every cell was assigned its relevant velocity head $\frac{v^2}{2g}$, pressure head $\frac{P}{\rho g}$, and magnitude of the z coordinate using ParaView's calculator option. The total head at both locations is then given by equation (4.1). The efficiency of the energy dissipation η is found using equation (4.2).

$$\mathbf{E} = \mathbf{z} + \frac{\mathbf{P}}{\rho \mathbf{g}} + \frac{\mathbf{v^2}}{\mathbf{2g}} \tag{4.1}$$

$$\eta = \frac{E_{in} - E_{out}}{E_{in}} \times 100\% \tag{4.2}$$

Figure 4.9: Energy change across the baffle drop shaft for 24 l/s

The datum was fixed to the bottom slab/floor of the baffle drop shaft. In a global perspective, energy at the inlet is mainly potential energy, and the energy at the outlet energy is dominated by kinetic energy. For all of the configurations, free-surface flows were evident along the entrance channel and the outlet tunnel. Inlet and outlet energy were extracted and integrated to calculate the average energy of that particular section using an energy distribution diagram. Using (4.2), the

efficiency of energy dissipation for different model configurations were obtained and plotted with respect to the non dimensional discharge of Q* ($Q/\sqrt{(gH^5)}$) as shown in Figure 4.10.

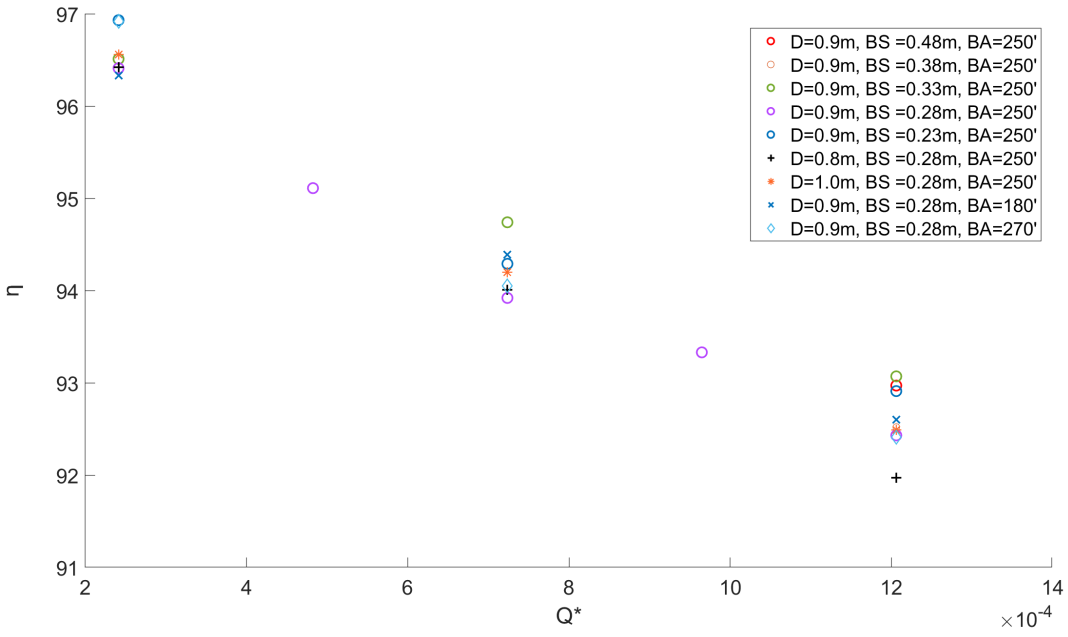

Figure 4.10: Energy dissipation efficiency as a function of Q^* for different geometric configurations

With increasing discharge, the baffle drops shaft's energy dissipation efficiency declined in agreement with previous studies on other types of baffle drop shafts. η values ranged from roughly 92% to 97%. for free flow conditions.

A base case configuration was also considered for the parametric analysis by removing all the baffles for a 0.9 m shaft diameter. Energy dissipation efficiency was found to be 91%. This value agrees with those found by Rajarathnam (2017) [11]. This efficiency is only achieved only if the outlet channel maintains a free surface flow condition. The maximum discharge in this study was 40 l/s with a clear free surface flow evident at the outlet.

There is no clear correlation between the baffle spacing, shaft diameter, and baffle rotation angle of the baffle dropshaft and the efficiency of energy dissipation. Therefore, when choosing those geometric characteristics and optimizing the structural design for a baffle dropshaft, other

important considerations such as air entrainment, pressure, and construction and maintenance costs should be taken into account.

4.3.2 Local energy dissipation

Figure 4.10 depicts global energy dissipation and does not demonstrate significant variation for different configurations. However, it is important to understand the local energy dissipation because the h/H ratio (baffle spacing/total height) can provide design engineers with some insights on how much of the total energy is being dissipated by the baffles for different flow rates. The flow conveyance of the baffle-drop shaft consists of numerous flow phenomena, including impact waves, circulating flows, and oscillating flows. The process of energy exchange in the drop shaft is extremely complex with these multiple criteria. To quantify the local energy dissipation of the baffle drop shaft, the average energy at the baffle edge was extracted as shown in Figure 4.11.

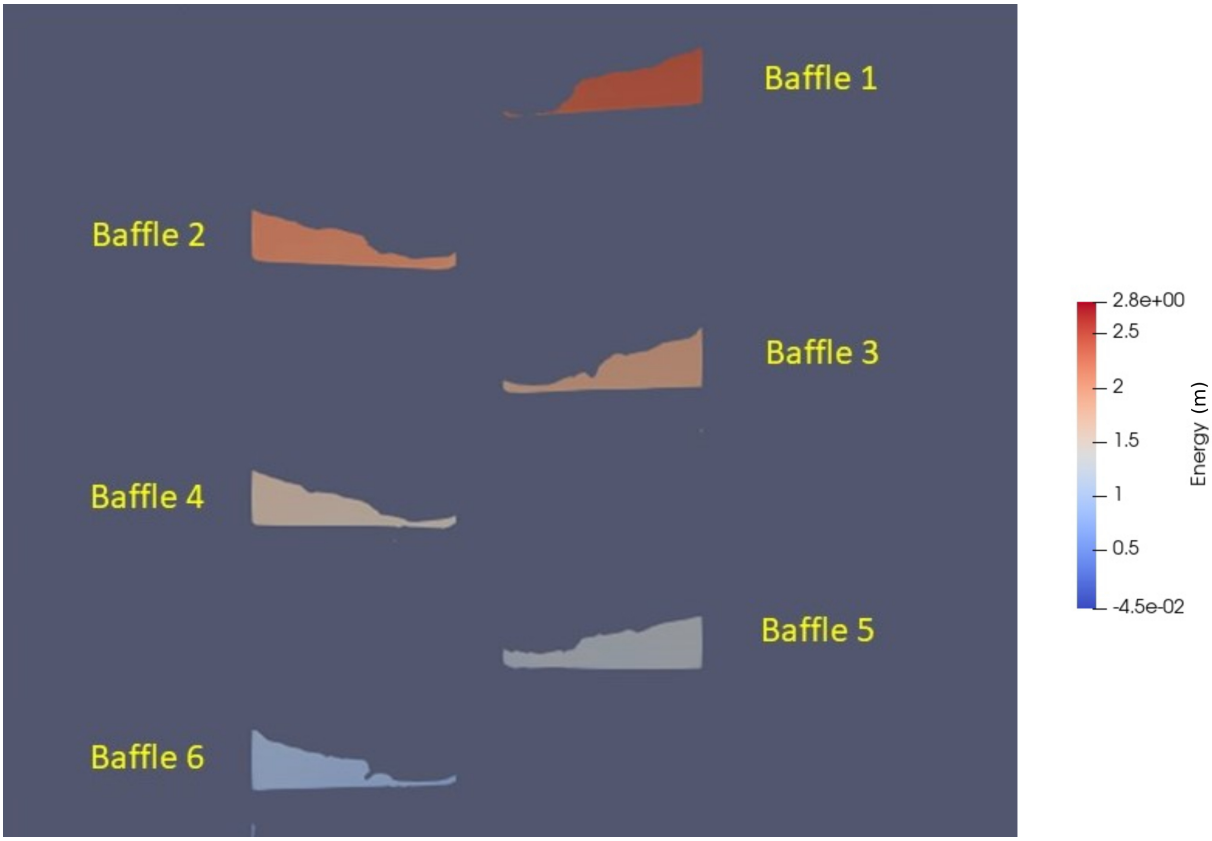

Figure 4.11: Energy head at edge of the baffle for 24 l/s for the benchmark geometry

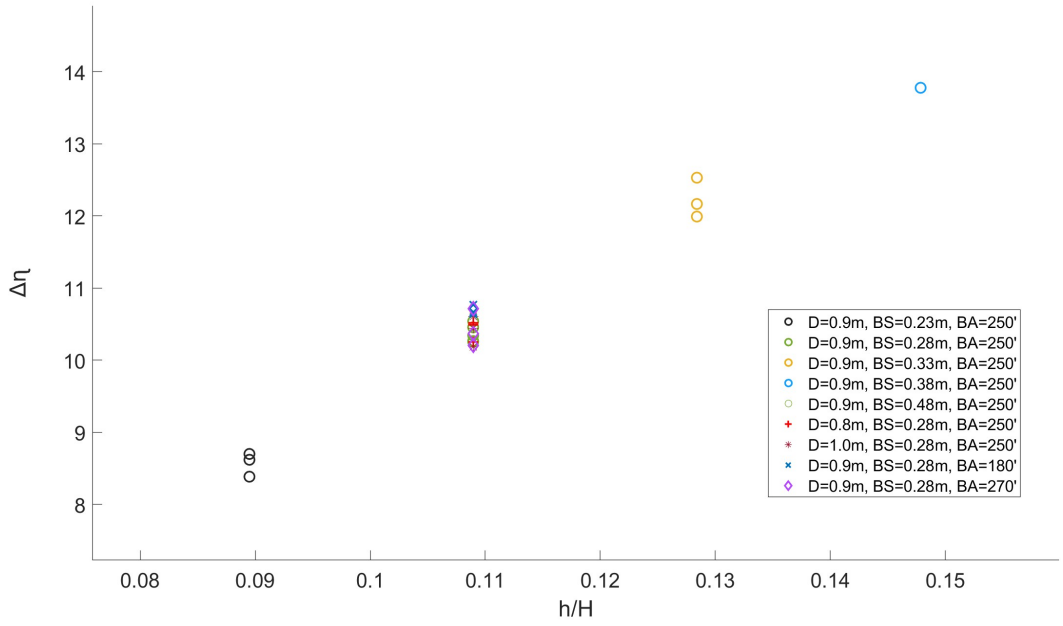

Figure 4.12: Efficiency of local energy dissipation versus h/H

The efficiency of local energy dissipation ($\Delta\eta$) is depicted in Figure 4.12. The energy dissipation that occues over every baffle drop is dependent on baffle spacing. Approximately, the same amount of energy is dissipated over every baffle drop regardless of the the shaft diameter and baffle rotating angle. Even though the global energy dissipation decreased as the discharge increased, the amount of local energy dissipation percentage depends mainly on the baffle spacing. The key point to note is that the total energy dissipated by the drop shaft may be distributed in a uniform manner along the drop shaft by using a suitable number of baffles that are spaced optimally.

The importance of energy dissipation of baffle drop shafts depend on the application. The number of baffles to be used may depend on the designer's judgment based on other criteria. Sometimes, baffle drop shafts need to accommodate higher discharge in sudden flood events. Because of the presence of baffles and the shaft wall, the water boundary layer cannot grow outward under high discharges. This study did not focus on such submerged flow conditions, because it changes the flow conditions inside the baffle drop shaft by converting the system into pressurized flow system with different boundary conditions. Due to its high velocity, water often enters the

pressurized drop shaft with higher amounts of kinetic energy. Friction and turbulent energy loss is the main energy dissipation mechanism in a pressurized system.

4.4 Baffle pressure

We find that there is no significant impact on energy dissipation by minimizing or maximizing the baffle geometry, but the baffle spacing may help to avoid excessive pressure on the baffles. Due to increased flow rates, the time-averaged pressure rises with increasing discharge on the baffles in all configurations.

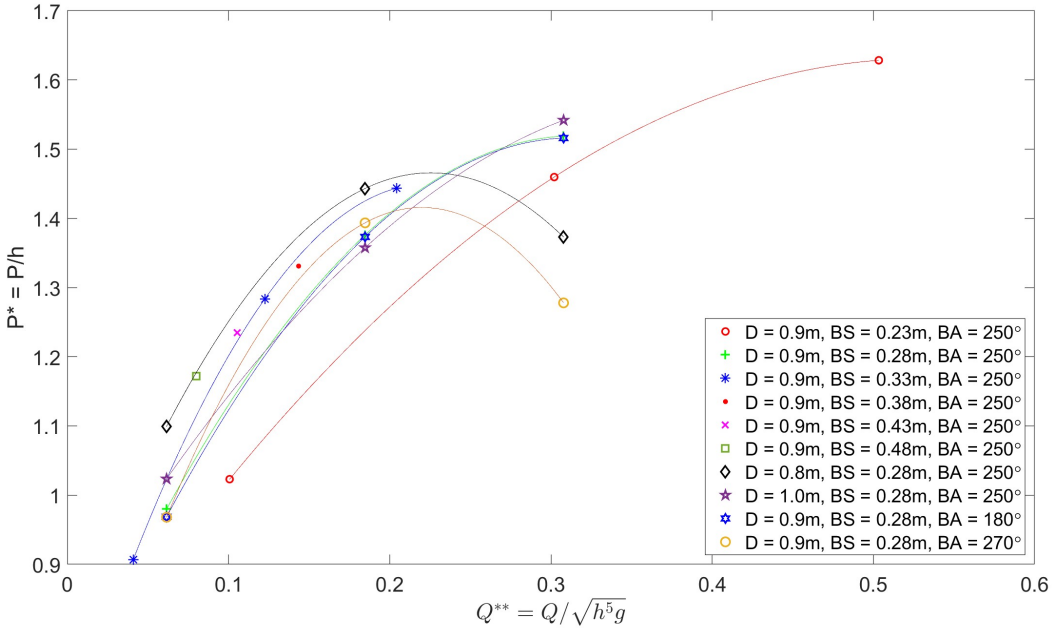

Figure 4.13: Maximum pressure distribution for different geometric configuration

Figure 4.13 depicts the variation of maximum pressure that is experienced by the baffles. Maximum baffle pressure is directly proportional to the baffle spacing until baffles become fully submerged. Maximum pressure starts to decrease at a certain point because the depth of the water cushion on the baffle at higher discharges. Generally, till Q^{**} = 0.21 pressure increases for all the simulations and then starts to vary based on the other geometric parameters. Residence time

of the water on the baffle increases with baffle rotating angle due to higher travel length, which creates a much higher water cushion on the baffle. Impact force decreases with the water depth underneath the baffle; hence, pressure can decrease by increasing baffle angle. Q^{**} can be decreased by increasing baffle spacing, but cost-wise, it might be better to use a smaller number of baffles. If the baffle drop shaft is to accommodate a much higher discharge, the best option for the designer is to increase the baffle spacing while focusing on the maximum pressure that can be safely accommodated from a structural point of view for that particular baffle spacing.

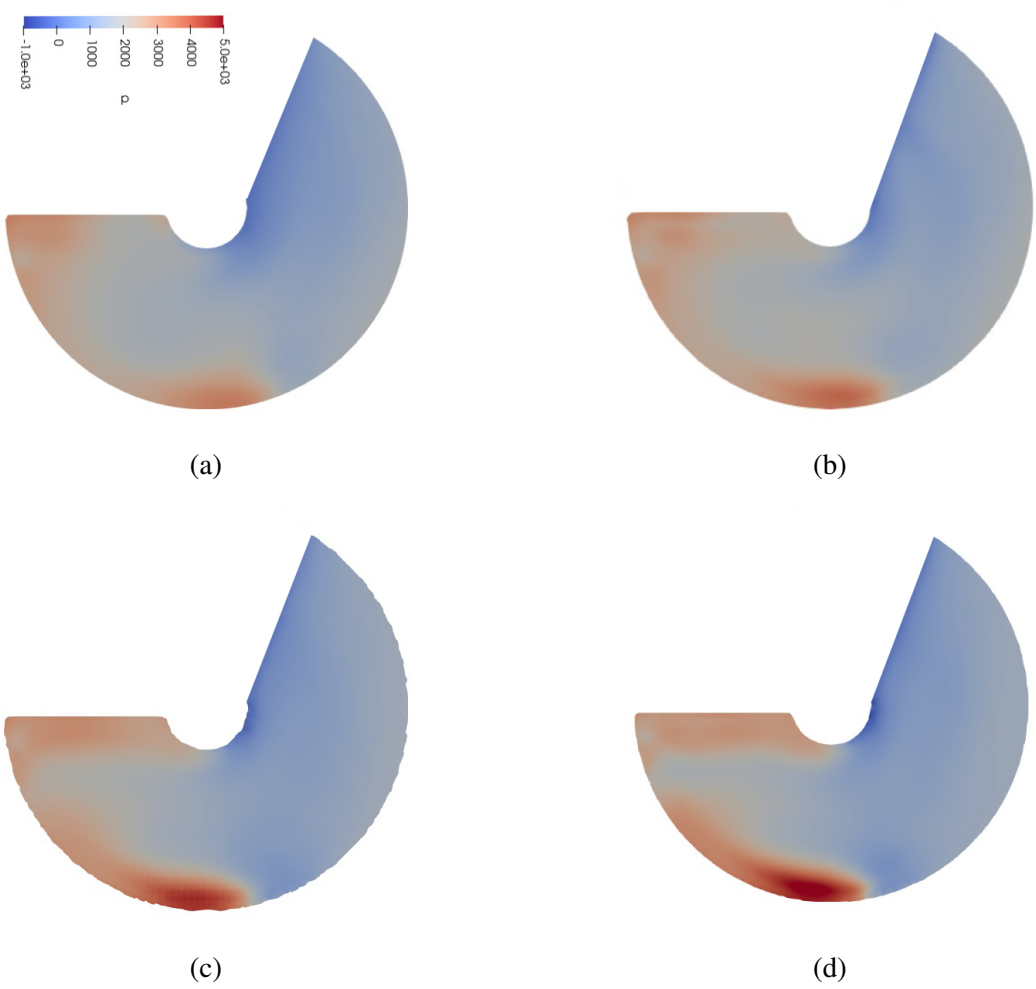

Figure 4.14: Pressure distribution (in Pa) on the baffle for maximum flow condition (40 l/s) (a) Baffle Spacing = 0.23 m (b) Baffle Spacing = 0.28 m (c) Baffle Spacing = 0.38 m (d) Baffle Spacing = 0.48m

.

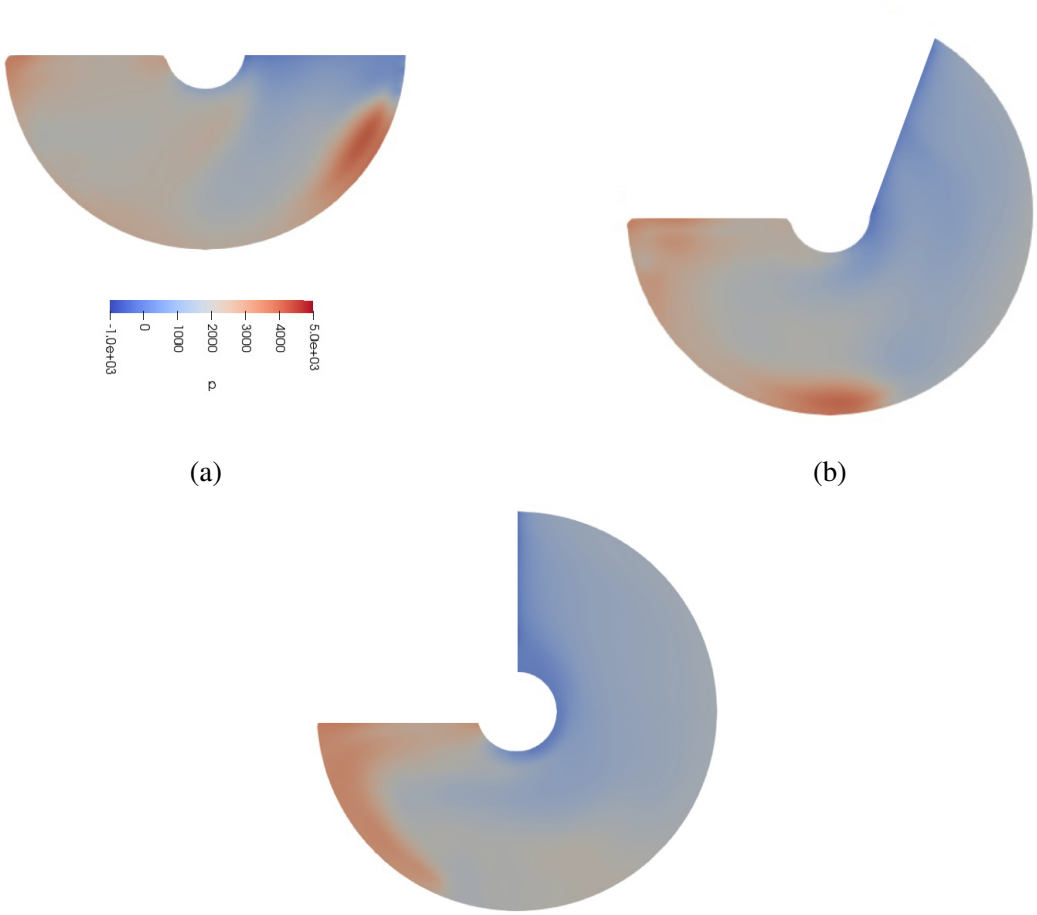

(a) (b)

(c)

Figure 4.15: Pressure distributions (Pa) on a baffle for maximum flow condition (40 l/s) with baffle rotating angle a)$\theta = 180^\circ$ b) $\theta = 250^\circ$ c) $\theta = 270^\circ$

Pressure distributions on the baffles is a good indicator for structural designers to identify areas that experience higher pressure based on the geometry of the baffle drop shaft. Since baffles are structural elements that are prone to damage quickly, it is important to minimize pressure loads on the baffle due to the impact of caused by falling water jets. Figures 4.14 - 4.16.

According to the Figure 4.14-Figure 4.16, maximum pressure can be observed at the water jet impact location. Considering rotary flow inside the baffle drop shaft, maximum pressure occurred near the outer wall, hence additional reinforcement can be provided in that area by the designer. Hydro static pressure is slightly higher near the blocking wall due to rolling of the flow.

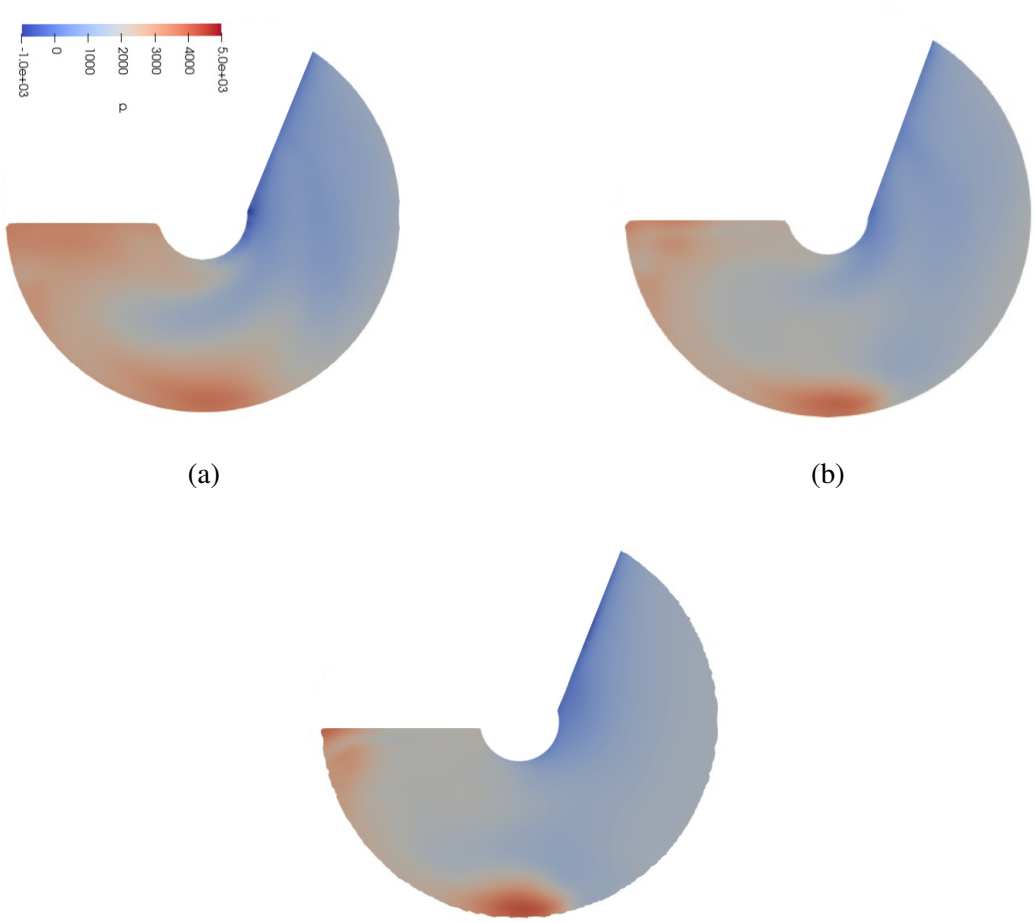

(a) (b)

(c)

Figure 4.16: Pressure distribution (Pa) on the baffle for maximum flow condition (40 l/s) with shaft diameter a) Shaft Diameter(D) = 0.8m b) Shaft Diameter(D) = 0.9m c) Shaft Diameter(D) = 1.om

4.5 Bulking

It is known that air is entrained in the baffle drop shaft due to flow drop and turbulence. This can be mitigated by installing air windows that sustain air equilibrium in the shaft. Air entrainment must be evaluated to determine if a deaeration chamber is required or if the operating capacity of the drop shaft must be decreased to reduce the air entrainment rate. The volume of flow expands due to high air entertainment. Quantifying the air entrainmenis a difficult problem.Here a bulking factor is defined as follows:

$$\text{Bulking factor} = \frac{\textbf{Flow volume between two baffles}}{\text{Available space between two baffles}}$$

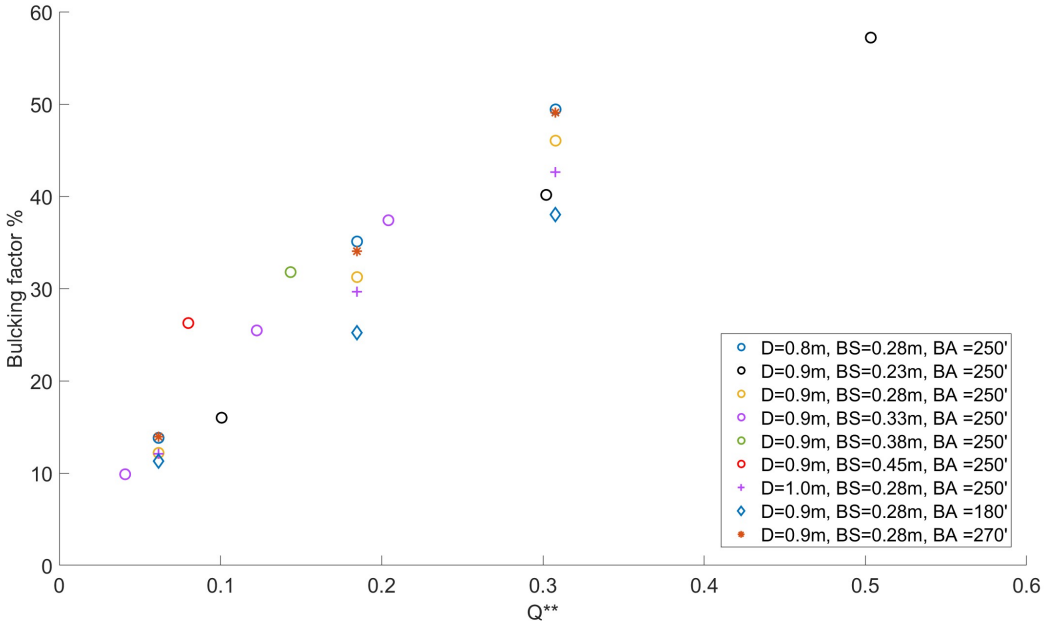

Figure 4.17: Bulking factor versus Q^{**}

Bulking increases with discharge because it creates high turbulence conditions in the baffle drop shaft. The lowest bulking factor can be observed in the 180^0 baffle configuration due to low air entrainment, and higher bulking can be observed at higher baffle spacing. Less shaft diameter also increases the bulking effect due to less available volume between two baffles. Lesser bulking

factor is one indication that configuration can accommodate much higher discharge using that particular geometry. Figure 4.18 shows that baffles are partially submerged.

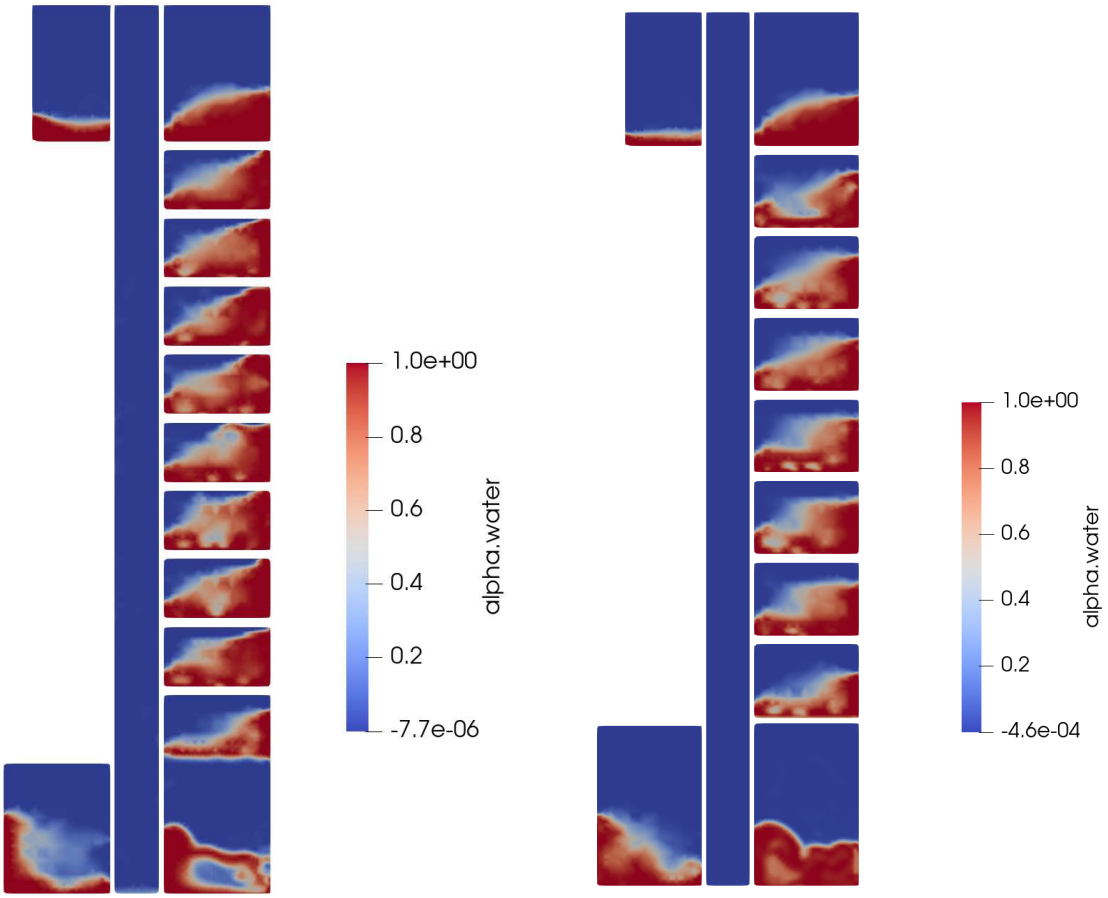

(a) (b)

Figure 4.18: Cross section perpendicular to y axis : (a) Alpha value distribution across the section - D = 0.9m, BS = 0.23m, and BA = 250^0 ; (b) Alpha value distribution across the section - D = 0.9m, BS = 0.28m, and BA = 250^0 .

Chapter 5

Conclusions and Recommendations

There is no systematic investigation that has been performed to evaluate the hydraulic performance of a baffle drop shaft with a block wall. In this study, flow through different geometries of baffle drop shafts (Type 2) were investigated from energetic and dynamic perspectives. The type 2 baffle drop shaft is special because of its unique geometry mainly due to the block wall that acts as a vertical barrier while the baffle blocks the horizontal movement of the flow. This chapter provides some conclusions drawn from both the physical model and the CFD simulation studies. Some recommendations for future studies are also provided.

5.1 Conclusions

The physical model experiments at 1:10 scale of a baffle drop shaft (operated in conformance with the principles of Froude number similitude) yielded the following key findings.

1. Similar flow regimes were observed at each baffle, with almost equal pressure and velocities at the same locations on different baffles for different discharges. This repetitive flow profile is an indication that the baffle dissipates the similar amounts of energy for each baffle drop.

2. The impact of the falling flow on the baffle, rolling flow impact on the block wall, complex flow pattern due to turbulence, friction on the baffle and outer shaft and high air entrainment are the main energy dissipation mechanisms of this proposed baffle drop shaft. Efficiency of energy dissipation slightly decreases with the increase of Q^* but remains at a high level. η varies from 89.6%to 91.9% under free flow conditions, indicating that baffle drop shaft is a excellent energy dissipator.

3. Based on visual observations, air entrainment is significantly higher for higher discharges. The water flowing from the upper baffle impacts the water cushion below, and the subsequent

rolling water causes a lot of air bubbles to be mixed in. The air entrainment increases energy dissipation.

The CFD model of a baffle drop shaft with at a 1:10 scale was used to perform a parametric study. RANS realizable k-ϵ was selected as a turbulence model because of its versatility and ability to simulate the details of complex flow. OpenFOAM was selected as the numerical solver, and the VOF method was used to track the surface between air and water. The following conclusions can be made from the study:

1. The energy dissipation of flow through the baffle drop shaft was investigated from both global and local perspectives. Global energy dissipation efficiency was found to be greater than 91% for different geometric configurations. Shaft diameter, baffle spacing, and baffle rotating angle have less influence on global energy dissipation. The percentage of local efficiency of energy dissipation on the baffle drop shaft increases with baffle spacing. Energy dissipation helps minimize the potential for erosion, turbulence, and excessive pressure buildup.

2. The drop shaft must be robust enough to bear the resulting impact forces and hydraulic pressures from the falling fluid. Maximum baffle pressure is directly proportional to the baffle spacing and discharge.

3. Air entrainment can be significant in baffle drop shafts. Provision of an air vent helps to exchange the air between water and the atmosphere without pressurizing the system. Air entrainment increases with discharge and baffle spacing. Better CFD models and techniques are required to quantify the air entrainment in a more reliable manner.

5.2 Recommendations for future research

Further work is required to investigate the different possible flow modes that can exist in a baffle drop shaft under extreme discharge conditions. Furthermore, there is a need to explore

the effects of air entrainment using different CFD approaches in conjunction with physical models. These are areas for future research on this topic.

Bibliography

[1] Yongfei Qi, Yurong Wang, and Jianmin Zhang. Three-dimensional turbulence numerical simulation of flow in a stepped dropshaft. *Water (Switzerland)*, 11, 12 2018.

[2] Xi chen Wang, Jian Zhang, Zong fu Fu, Hui Xu, Ting yu Xu, and Chen lu Zhou. Influences of flow rate and baffle spacing on hydraulic characteristics of a novel baffle dropshaft. *Water Science and Engineering*, 13(3):233–242, sep 2020.

[3] Esteban Guerrero, Felipe Muñoz, and Nicolás Ratkovich. Comparison between eulerian and vof models for two-phase flow assessment in vertical pipes. *CTyF - Ciencia, Tecnologia y Futuro*, 7:73–84, 2017.

[4] H. Chanson. Hydraulics of roman aqueducts: Steep chutes, cascades, and dropshafts. *American Journal of Archaeology*, 104:47–72, 1 2000.

[5] Huan Liu, Yangwen Jia, and Cunwen Niu. "sponge city" concept helps solve china's urban water problems. *Environmental Earth Sciences*, 76:1–5, 2017.

[6] Qinghua Yang and Qian Yang. Experimental investigation of hydraulic characteristics and energy dissipation in a baffle-drop shaft. *Water Science and Technology*, 82:1603–1604, 10 2020.

[7] A. Jacob Odgaard, Troy C. Lyons, and Andrew J. Craig. Baffle-drop structure design relationships. *Journal of Hydraulic Engineering*, 139:995–1002, 9 2013.

[8] SH Anderson. Model studies of storm-sewer drop shafts. 1961.

[9] Nancy Schultz, Don Del Nero, Sharon Matthews-Rohadfox, and Eric Lane Glover. Lessons learned from operating large sewage tunnels. *Proceedings of the Water Environment Federation*, 2012:98–121, 2014.

[10] Robert Andoh, Kwabena Osei, Jeremy Fink, and Mike Faram. Novel drop shaft system for conveying and controlling flows from high level sewers into deep tunnels. *World Environmental and Water Resources Congress 2008: Ahupua'a - Proceedings of the World Environmental and Water Resources Congress 2008*, 316, 2008.

[11] Yiyi Ma, David Z. Zhu, and Nallamuthu Rajaratnam. Air entrainment in a tall plunging flow dropshaft. *Journal of Hydraulic Engineering*, 142:04016038, 2016.

[12] Pardeep Kumar and R. P. Saini. Study of cavitation in hydro turbines-a review. *Renewable and Sustainable Energy Reviews*, 14:374–383, 2010.

[13] Sean Mulligan, Stephen Nash, and Eoghan Clifford. Vortex drop shaft structures : State-of-the-art and future. 2019.

[14] Jie Yi Shen, Jian Hua Wu, and Fei Ma. Hydraulic characteristics of stepped spillway dropshafts. *Science China Technological Sciences*, 62:868–874, 5 2019.

[15] A. Margevicius. No title. 2009.

[16] Qinghua Yang and Qian Yang. Numerical investigation of the turbulence characteristics and energy dissipation mechanism of baffle drop shafts. *Water Science and Technology*, 83:2259–2270, 5 2021.

[17] N. Rajaratnam, A. Mainali, and C. Y. Hsung. Observations on flow in vertical dropshafts in urban drainage systems. *Journal of Environmental Engineering*, 123(5):486–491, 1997.

[18] Gaetano Crispino, Pasquale Contestabile, Diego Vicinanza, and Corrado Gisonni. Energy head dissipation and flow pressures in vortex drop shafts. *Water (Switzerland)*, 13, 2021.

[19] Pfister Michael and Chanson Hubert. Two-phase air-water flows : Scale effects in physical modelling. 26:291–298, 2014.

[20] Andreas A Aigner. Navier-stokes equation. 2020.

[21] H K Versteeg and W Malalasekera. An introduction to computational fluid dynamics second edition.

[22] Mukhtar Abdulkadir. Experimental and computational fluid dynamics (cfd) studies of gas-liquid flow in bends, 2011.

[23] Dendy. Adanta, Rizwanul. Fattah, and Nura Muaz. Muhammad. Comparison of standard $k-\epsilon$ and sst $k-\omega$ turbulence model. *Mechanical Science and Engineering*, pages 39–44, 2020.

[24] Erdinc Sogut, Deniz Velioglu Sogut, and Ali Farhadzadeh. A comparative study of interaction of random waves with a cluster of structures on a berm with rans and les models. *Coastal Engineering*, 168:103941, 2021.

[25] Eyub Canli, Ali Ates, and Sefik Bilir. Comparison of turbulence models and cfd solution options for a plain pipe. *EPJ Web of Conferences*, 180, 2018.

[26] Zhongdong Qian, Xiaoqing Hu, Wenxin Huai, and António Amador. Numerical simulation and analysis of water flow over stepped spillways. *Science in China, Series E: Technological Sciences*, 52:1958–1965, 2009.

[27] Jian Min Zhang, Jian Gang Chen, Wei Lin Xu, Yu Rong Wang, and Gui Ji Li. Three-dimensional numerical simulation of aerated flows downstream sudden fall aerator expansion-in a tunnel. *Journal of Hydrodynamics*, 23:71–80, 2011.

[28] H. Kheirkhah Gildeh, A. Mohammadian, I. Nistor, and H. Qiblawey. Numerical modeling of turbulent buoyant wall jets in stationary ambient water. *Journal of Hydraulic Engineering*, 140:04014012, 2014.

[29] Paola Elizabeth Rodríguez-Ocampo, Michael Ring, Jassiel Vladimir Hernández-Fontes, Juan Carlos Alcérreca-Huerta, Edgar Mendoza, and Rodolfo Silva. Cfd simulations of multi-phase flows: Interaction of miscible liquids with different temperatures. *Water (Switzerland)*, 12, 2020.

[30] Rupak Biswas and Roger C. Strawn. Tetrahedral and hexahedral mesh adaptation for cfd problems. *Applied Numerical Mathematics*, 26:135–151, 1998.

[31] Mohammad Reza Haghgoo. A comparison of cfd software packages to find the suitable one for numerical modeling of gasification process. 898:1–27, 2013.

[32] Mohammad Manafpour and Hamzeh Ebrahimnezhadian. The multiphase capability of openfoam cfd toolbox in solving flow field in hydraulic structure. *4th International Conference on Long-Term Behavior and Eco-Friendly Dams*, pages 323–330, 2017.